Unravelling physiological signatures of tomato bacterial wilt and xylem metabolites exploited by Ralstonia solanacearum

Léo Gerlin, Antoine Escourrou, Cédric Cassan, Felicià Maviane Macia, Nemo Peeters, Stéphane Genin, Caroline Baroukh

Unravelling physiological signatures of tomato bacterial wilt and xylem metabolites exploited by *Ralstonia solanacearum*

Léo Gerlin[1], Antoine Escourrou[1], Cédric Cassan[2,3], Felicià Maviane Macia[1,4], Nemo Peeters[1,4], Stéphane Genin[1*], Caroline Baroukh[1]*

[1]LIPM, Université de Toulouse, INRAE, CNRS, Castanet-Tolosan, France

[2]UMR BFP, Université de Bordeaux, INRAE, 33882 Villenave d'Ornon, France

[3]Bordeaux Metabolome, MetaboHUB, PHENOME-EMPHASIS, 33140 Villenave d'Ornon, France

[4]Toulouse-Plant-Microbe-Phenotyping TPMP PHENOTOUL PHENOME-EMPHASIS LIPM, Université de Toulouse, INRAE, CNRS, Castanet-Tolosan, France

*For correspondence:

Postal address: Caroline Baroukh, Laboratoire des Interactions Plantes-Microorganismes, 24 chemin de Borde Rouge – Auzeville, CS 52627, 31326 CASTANET TOLOSAN CEDEX, France

Email: caroline.baroukh@inrae.fr;

Tel.: (+33) 5 61 28 55 25;

Keywords: metabolism, plant pathogen, transpiration, growth, glutamine, putrescine, NMR, metabolomics, automated phenotyping

Running title: Xylem metabolites exploited during bacterial wilt

Originality-Significance Statement.

The plant pathogen *Ralstonia solanacearum* colonizes plant xylem vessels, reaching 10^{10} colonies per gram of plant. To proliferate so dramatically and thwart host responses, the nutritive resource supply is central to successful infection, but is still poorly understood. Through a combination of automated phenotyping, quantitative metabolomics and genetic approaches, we identify on the one hand sensitive markers of the infectious process and on the other hand nutritional substrates that allow the rapid growth of the pathogen in vascular tissues. In particular, we show that during bacterial colonization, xylem is depleted in two amino acids abundantly present: glutamine and asparagine. In addition, we show that sugars have little role to sustain growth of the pathogen and progression of the disease, using a mutant unable to catabolize glucose, sucrose and fructose. These findings challenge the classical view that the pathogen's infection process depends on abundant sugars in plants to colonize xylem. Furthermore, the monitoring of plant physiological markers during infection reveals that the phase of amino acid assimilation and simultaneous bacterial proliferation corresponds to a tipping point of the infection, associated with a strong alteration of plant physiology including growth arrest and transpiration arrest.

Summary

The plant pathogen *Ralstonia solanacearum* uses plant resources to intensely proliferate in xylem vessels and provoke plant wilting. We combined automatic phenotyping and tissue/xylem quantitative metabolomics of infected tomato plants to decipher the dynamics of bacterial wilt. Daily acquisition of physiological parameters such as transpiration and growth were performed. Measurements allowed us to identify a tipping point in bacterial wilt dynamics. At this tipping point, the reached bacterial density brutally disrupts plant physiology and rapidly induces its death. We compared the metabolic and physiological signatures of the infection to drought stress, and found that similar changes occur. Quantitative dynamics of xylem content enabled us to identify glutamine (and asparagine) as primary resources *R. solanacearum* consumed during its colonization phase. An abundant production of putrescine was also observed during the infection process and was strongly correlated with *in planta* bacterial growth. Dynamic profiling of xylem metabolites confirmed that glutamine is the favored substrate of *R. solanacearum*. On the other hand, a triple mutant strain unable to metabolize glucose, sucrose and fructose appears to be only weakly reduced for *in planta* growth and pathogenicity.

Introduction

The *Ralstonia solanacearum* species complex (RSSC) includes a diverse group of pathogenic strains, causative agents of bacterial wilt on many plants (Álvarez et al., 2010; Hayward, 1991). These strains were classified in four main evolutionary lineages also called phylotypes (Fegan & Prior, 2005) which were recently assigned to three distinct species (Prior et al., 2016; Safni et al., 2014). The bacterial wilt disease caused by RSSC strains on tomato results from a multi-stage infection process in which, after the root infection stage and colonization of the root cortex tissues, bacteria invade the xylem vessels. This allows their spread to the aerial part of the plant, concomitantly with a strong multiplication (Caldwell et al., 2017; Vasse et al., 1995; Xue et al., 2020). High population density in the xylem vessels, along with the production of exopolysaccharide (EPS), reduces the sap flow leading to the appearance of wilting symptoms (Hikichi et al., 2017). Resistance of the plant to limit bacterial colonization proceeds at different steps including root invasion (Morel, Guinard, et al., 2018; Poueymiro et al., 2009), vertical movement upwards to the stem, and vessel to vessel diffusion in the xylem (Caldwell et al., 2017; Planas-Marquès et al., 2020; Xue et al., 2020). On the other hand, *R. solanacearum* spp. relies on effectors delivered by the type-three secretion system to circumvent plant immunity (Landry et al., 2020) as well as many other virulence factors which contribute to pathogenic fitness at the different infection steps (Genin & Denny, 2012; Hikichi et al., 2017).

Once in xylem vessels, *R. solanacearum* spp. reaches massive bacterial density up to 10^{10} colony forming units (CFU) per g of fresh stem (Lowe-Power, Khokhani, et al., 2018; Perrier et al., 2019). Therefore, bacterial infection success is highly dependent on the rapid assimilation of nutrients to sustain both production of biomass (proliferation) and factors subverting host immunity (virulence) (Lowe-Power, Khokhani, et al., 2018). There is evidence for intertwined regulation between virulence genes and metabolic genes (Khokhani et al., 2017; Peyraud et al., 2016, 2018), but how metabolic resources are acquired *in planta* remains poorly understood. A recent study, however, showed that sap

from infected plants is enriched in several nutrients that improve *R. solanacearum* growth in sap (Lowe-Power, Khokhani, et al., 2018), notably sucrose (Hamilton et al., 2021).

The consumption of host resources associated with intense bacterial proliferation, as well as the effects of virulence factors, should induce strong alterations of the plant physiology. In the case of bacterial wilt, only qualitative observations of wilting are usually made, and little is known about these physiological alterations in terms of dynamic and quantitative data. The progression of the disease is generally evaluated by a disease index (i.e a visual scoring of the wilting symptoms) or by counting of the bacterial population extracted from infected plants. Although the latter method appears more sensitive for monitoring the course of the disease, it sometimes happens that the bacterial load is not correlated with disease symptom progression (Angot et al., 2006; Lebeau et al., 2011).

In this study, we aimed at quantifying the dynamics of the bacterial wilt disease on tomato plants in greenhouse conditions, using *Ralstonia pseudosolanacearum* GMI1000 (Salanoubat et al., 2002), a model strain representative of the RSSC. We used automated plant phenotyping and metabolomics of both xylem sap and plant organs to determine the evolution of various physiological parameters at different stages of xylem vessels colonization. This quantitative kinetic study unraveled a critical point in the *R. solanacearum* colonization process beyond which the host-pathogen interaction switches to the side of the disease, with strong physiological effects on the plant and a rapid progression of symptoms. In a 48h window after infection, the pathogen drains the major substrates allowing for its strong proliferation. Quantitative metabolomics of infected xylem confirmed that putrescine concentration is a relevant marker of the infection process and strongly suggested that glutamine and asparagine are the major carbon sources sustaining bacterial proliferation *in planta*. On the other hand, the generation of a triple mutant strain defective for the assimilation of glucose, sucrose and fructose revealed that these sugars play little role in sustaining pathogen's growth *in planta*, as evidenced by the phenotype of this strain on tomato plants.

Results

High-throughput phenotyping of tomato plants during bacterial wilt

To evaluate the physiological and metabolic parameters associated with the infection of *R. solanacearum* strain GMI1000 of its tomato host, we monitored the progression of the bacterial wilt symptoms over 9 days in a controlled conditions greenhouse using an automated high-throughput plant phenotyping facility (http://tpmp.inrae.fr). To improve the synchronization of plant infection, the inoculation was carried out on root-damaged plants by soil drenching with a suspension of 5.10^6 CFU/ml. Control plants (hereafter referred to as 'healthy plants') were inoculated with water only. Two independent experiments comprising respectively 90 and 81 plants were performed. Each experiment was analyzed separately (automatic phenotyping, metabolomics) and a similar response profile was observed for both. The data presented in the following sections correspond to an experiment (three replicates, 81 plants with 63 infected / 18 healthy); the data of the second experiment are presented in Fig. S4, Fig. S6, Table S1. A larger number of infected plants was monitored given the greater variability expected in the case of the interaction with the pathogen. Automated phenotyping included weighing for the estimation of transpiration and imaging. Analysis of acquired images (Fig. S1) allowed to estimate the position (vertical) of the plant center of gravity (Fig. S2 and Fig. S3) and the chlorophyll content (Liang et al., 2017). Plants were also manually sampled at different days post inoculation (1, 3, 4, 5, 7, 8) to determine organ fresh/dry weight, as well as organ and xylem biochemical profiling and bacterial population (CFU). The appearance of bacterial wilt symptoms, from 0 (no symptoms) to 4 (complete wilting) (Arlat & Boucher, 1991) was also followed.

R. solanacearum alters the plant physiological balance rapidly after infection

Figure 1

Physiological dynamics of the disease progression clearly revealed a tipping point in plant physiology and infection kinetic. In our experimental conditions, this point is at 4 dpi and corresponds to a colonization stage of 10^8 bacterial colonies per g of FW (Figure 1). Before this tipping point, plant general physiology remains similar between healthy and infected individuals: growth/transpiration rates, chlorophyll content/center of gravity vertical position estimation (Figure 1, Figure 2). At 4 dpi, transpiration begins to decrease significantly for infected plants, indicating that bacterial colonization is starting to affect plant physiology in a detectable way, although symptoms are barely visible (50% of plants at disease index 0). Early impact on transpiration was expected as xylem occlusion limits the transmission of water to aerial parts. This very early stage of symptom development shows that before disease index score 2 the plant has already been strongly colonized by bacteria. Position of the plant center of gravity, which is a proxy of how upwards the plant is growing, is also significantly affected (Figure 2) at 4 dpi. Some physiology parameters such as plant growth and chlorophyll content were impacted later and correlated with disease symptom appearance (disease index of 1 and above). From 5 dpi only, plant growth began to slow down for infected plants and chlorophyll content started to decrease, further showing that a major transition occurred around 4 dpi. We will refer below to this major transition as the "tipping point".

After this tipping point, infected plants almost stopped growing: the growth rate was 0.044 d^{-1} for infected plant versus 0.2126 d^{-1} for healthy plants between 4 and 8 dpi. Transpiration also strongly decreased, from nearly 100 mL to less than 10 mL per day, while it reached around 200 mL per day for larger healthy plants. Furthermore, the fastest bacterial proliferation was observed around the tipping point (bacterial growth rate of 0.09 h^{-1} between 3 and 5 dpi), before slowing down (bacterial growth rate of 0.02 h^{-1} between 5 and 8 dpi). It indicated that the first colonization stage in xylem vessels is a fast proliferation of *R. solanacearum* with limited visible impacts (symptoms) but which induces a major shift in plant physiology. After this shift, bacterial proliferation slows down as the

high-density population of the pathogen begins to become a burden to plant development. This is probably due to lack of nutrients because of plant stopped growth.

Figure 2

Tomato organ-specific changes induced by the bacterial wilt disease

Fresh and dry weights of healthy and infected plant organs were used to determine the impact of *R. solanacearum* proliferation on plant water status (Figure 3A). Organ water content remains constant for healthy plants. As expected from our transpiration results (Figure 1), the percentage of water in infected plants decreased during bacterial infection for leaves and stems. Organ dehydration was observed close to the previously defined tipping point (a detachment is observed at 4 dpi, although it is significant only at 5 dpi), almost simultaneously to the onset of transpiration deficiency (as observed in Figure 1), and close to the appearance of wilting symptoms (disease index). For roots, water content was in a similar range for infected and healthy plants, confirming that major bacterial proliferation in xylem vessels does not affect root hydration (Lowe-Power, Khokhani, et al., 2018). At later infection stage (7 and 8 dpi), corresponding to a disease index score of 3 (75% of the plant wilted) with plant transpiration close to 0 mL/day, leaves and stems remained however well-hydrated, only decreasing from 87% to 80% water and 95% to 92%, respectively.

Plant dehydration is suspected to affect central metabolism as high-water supply is essential for photosynthesis as well as for plant development/growth since water is necessary to constitute the turgor pressor. We thus performed quantitative metabolomics of plant tissues at 3, 5 and 7 dpi (Figure 3B, Fig. S5), to analyze different steps of the infection process. We did not find significant differences at 3 and 5 dpi. At 7 dpi, a drastic and significant impact on leaf and stem starch was observed (Figure 3B). In leaves, the proportion of starch was high in healthy plants (8.58 ± 6.06 %) while it was depleted in infected plants (0.08 ± 0.12 %). Amino acids also decreased significantly but less drastically. In accordance with the chlorophyll drop as deduced from image analysis (Figure 2), the quantification of chlorophyll content in leaves also seems to decrease in infected tissues but not significantly.

Figure 3

The bacterial wilt disease modifies metabolite availability in tomato xylem sap

We investigated further how *R. solanacearum* is able to proliferate intensely in xylem vessels by determining the carbon sources supporting bacterial proliferation in xylem sap. We extracted xylem sap of infected and healthy plant at different dpi for quantitative analysis NMR (see Materials and Methods). To assess which xylem metabolites are affected by infection, we performed a PCA. This multivariate analysis revealed that two principal components (PCs) explained 65% of the variability (see Fig. S7), on which we focused our analysis. Each individual point plotted in Figure 4A corresponds to a xylem sap sample (15 metabolites concentrations) transformed into the two uncorrelated PCs and associated with the corresponding bacterial population. We found that the first PC (explaining 30% of the variability) is not correlated with infection stage and reveals an important variability between plants independent of the infection. However, the second PC (explaining 25% of the variability) is strongly associated with the bacterial population level. Interestingly, uninfected xylem samples have very similar metabolic profiles as all the points are clustered whereas infected samples display a scattered profile. This suggests that impact of bacterial infection on xylem sap composition is heterogeneous between plants and that there is therefore a certain level of variation at this stage.

We plotted the contribution of the variables (metabolite concentrations) to the two PCs in Figure 4B. Variables differing most from zero on the horizontal axis (e.g ethanol, lysine, phenylalanine and valine) have an important contribution to the first PC, which implies that for these compounds there is an important inter-plant variability not correlated to infection. Conversely, variables differing most from zero on the vertical axis contribute to the second PC and are therefore associated with the bacterial population level. High levels of asparagine and glutamine (bottom of the plot) are associated to healthy plants and plants with low bacterial population, while high levels of putrescine and acetate are

associated with high bacterial population (see complete list in Table 1). We found that for healthy plants, concentrations are constant between 1 and 8 dpi (no statistical differences observed between sampling days, and no apparent temporal dynamics) so we determined a global mean for each plant (Table 1, Table S1). Glutamine appeared as the major component of xylem sap (75 percent of molar organic carbon) whereas the other compounds were found in much lower concentrations (sixteen times less at least).

Figure 4

Table 1

We found that the progression of the infection was associated with glutamine and asparagine decrease and provoked the appearance of putrescine (non-detectable in healthy plants) and an increase of acetate content. We also estimated that aspartate, phenylalanine, lysine, glutamic acid and leucine were not affected by *R. solanacearum* infection as the absolute loading weights are close to zero (inferior to 0.25). It was difficult to conclude firmly for the other variables as they were in an intermediate (and so less discriminating) area, between 0.25 and 0.75.

Dynamic profiling of tomato xylem fluid metabolites during *R. solanacearum* infection

Figure 5

PCA showed that some tomato xylem metabolites concentration vary during infection by *R. solanacearum*. In order to get a dynamic view of these changes, we monitored metabolite concentrations over several days in healthy and infected plants. The kinetic data for the 7 compounds with statistical differences for one time point or more are represented in Figure 5 (and in Fig. S8 for alanine). We noticed that statistical differences were mostly observed at 3, 4 or 5 dpi, certainly due to

a higher number of plants analyzed and sometimes high variability. For additional compounds tested, no statistical difference was observed (Fig. S8).

Putrescine was detected when plant infection resulted in high bacterial proliferation (between 3 and 5 dpi, see Figure 1) and its concentration stabilized in the last days of infection (7 and 8 dpi) when bacterial multiplication started to slow down. Putrescine therefore appears to be a sensitive and precise biomarker of the infection: its dynamics is strongly correlated with the onset and evolution of the bacterial wilt disease. Three other metabolites increase importantly and significantly in infected plants: 3-hydroxybutyric acid increases at 4 and 5 dpi, while it seems to decrease afterward, acetate increases from 4 to 7 dpi, and alanine (Fig. S8) seems to follow the same pattern than 3-hydroxybutyric acid.

Glutamine depletion is striking as the initial concentration (almost 3 mM) decreases to around 1 mM at the end of the sampling. Simultaneously, asparagine, which is observed at a smaller amount in healthy plants (around 1.5 mM) is also quickly depleted: our data indicate a drastic drop between 4 and 5 dpi. After this drop, asparagine concentration is around 0 (or at concentrations under the limit of detection). These parameters prove an intense metabolic activity over a short time window (48 hours) in xylem vessels, exactly around the tipping point of the infection previously reported (4 dpi).

Putrescine production is a reliable marker of *R. solanacearum* infection

Figure 6

The progression of bacterial wilt disease is usually monitored in two ways: either by disease index scoring or by enumerating bacteria extracted from infected tissues. We plotted the relationship between these two phenotypical markers and some of the physiological parameters we monitored during the infection assay: plant transpiration, putrescine production and glutamine concentration in xylem (Figure 6). The calculation of the regression coefficients (R^2) shows that these three markers are globally well correlated with the bacterial density (in $\log_{10}$ CFU/g of fresh weight) and the disease index, although we observe for the latter a greater dispersion of the points in the early stages of

infection. As expected, bacterial population best correlated with wilt symptom development (R^2 = 0.81 with disease index). Plant transpiration is an early marker of infection impact on plant physiology (Fig. 1) and accordingly a clear negative relationship was also observed with the bacterial population rate, confirming that bacterial proliferation has a strong negative impact on plant transpiration rate. It turned out that the bacterial population rate in xylem is also well correlated to the metabolic profile of infected xylem: positive correlation between putrescine concentration (in decimal logarithm) is high (R^2 =0.66), indicating that appearance and accumulation of putrescine is directly associated with R. *solanacearum* infection. Negative correlation with glutamine concentration is also significant but weaker (R^2 = 0.54).

Genetic evidence that sugars are not major carbon sources supporting growth of *R. solanacearum* in xylem

Figure 7

Xylem metabolomics revealed a significant decrease of glutamine over time as well as a negative correlation between bacterial density and glutamine content, whereas sugar content was found to not vary. To validate the hypothesis that *R. solanacearum* growth is mostly supported by glutamine and not sugars, we generated a triple mutant strain unable to uptake (and so metabolize) three major sugars found in plants: sucrose, glucose and fructose, glucose and sucrose being detected in our xylem content analysis. The strain GMI1000 glucose transport operon (RSp1632-RSp1635) was identified after screening a mutant library to identify genes essential for growth on glucose (Peyraud et al., 2018), but these genes were incorrectly annotated as a xylose transport system. Cumulative deletions in each sugar transport system were generated to create the mutant strain GRS941.We used *in vitro* growth assays on microplates to validate that strain GRS941 growth on sucrose (Figure 7A), glucose (Figure 7B) and fructose (Fig. S9) was severely impacted. We then performed automated phenotyping of strain GRS941 on tomato plants under conditions similar to those used for the wild-type strain. We observed

that growth *in planta* of strain GRS941 was similar to the wild-type and reached high population levels (Figure 7C). The transpiration rate was significantly lower for plants infected by GRS941 compared to the wild-type at 6 to 8 dpi, but the difference was small with a similar overall profile and an identical tipping point at 4 dpi (Figure 7D). Small but statistically significant variations of plant dry weight, disease index and imaging profiles were also observed (Figure 7, Fig. S9), but the mutant strain was still able to provoke full plant wilting symptoms. We therefore concluded that glucose, fructose and sucrose are not critical carbon sources sustaining the pathogen growth during the xylem infection stage, but rather complementary nutritive sources..

Discussion

In this study, we followed the dynamics of infection of the pathogen at the time of xylem colonization and its impact on plant physiology. Unlike several studies that have focused on the *R. solanacearum*-plant interaction using miniaturized in vitro pathosystems, we have conducted this work on 4-week old tomato plants grown in greenhouse conditions to get closer to *in natura* interactions. In order to synchronize the infection process, we carried out infections with scarified roots, enabling easier entry of bacteria into vascular tissues. This root wounding procedure made it possible to follow the infection kinetics with relatively homogeneous values of the measured parameters (see Figure 1, 2, 3, 5), contrary to what is observed with soil soaking inoculations where greater variability is observed (Morel, Peeters, et al., 2018). We used our experimental system to follow not only symptoms but also general growth and water status of the plant, as well as measure metabolites without a priori. We were then able for the first time to correlate them in a time series for a finer understanding of the overall process.

Physiological markers define a tipping point during of bacterial wilt infection.

The use of automated phenotyping has enabled us to collect many measurement points, thus allowing for a sensitive estimation of major parameters linked to the infection of tomato by *Ralstonia pseudosolanacearum*. In particular, our study reveals that markers such as the plant transpiration rate in plant tissue are excellent proxies to follow the progression of bacterial infection. Moreover, the comparison of the measurements in these standardized conditions show that the quantification of the bacterial load in planta, despite being destructive, is much more reliable than the rating of the symptoms by disease index which is still commonly used to follow the evolution of an infection (see Figure 6). The absence of visible symptoms is observed with plants already highly infected (up to 10^9 CFU per g of FW) and disease index scores of 0, 1 and 2 include very diverse *in planta* bacterial loads.

It is only when the disease index reaches 3 that the profiles become more homogeneous, but they correspond to an already very advanced stage of bacterial propagation and alteration of plant physiology. This emphasizes that disease index is a late marker of the infection process and some physiological markers such as the plant transpiration rate or vertical position of the center of gravity (proxy of how upwards the plant is growing) have a much better correlation with bacterial colonization.

The fine tracking of parameters (weight, transpiration, center of gravity, chlorophyll content) of the infection highlighted a specific step that we consider a tipping point beyond which the disease progresses to plant death. This tipping point corresponds to a stage where macroscopic disease symptoms are barely visible (disease index=0.5) and to the first detection of bacteria after extraction from plant tissues for counting (CFU per g of FW). This reveals that the plant can afford a load of bacteria in its vascular system before seeing its immunity overwhelmed by the pathogen, which is consistent with the observation of bacterial proliferation reaching 10^6 CFU per g of fresh weight in the resistant tomato plant cultivar Hawaii 7996 (Nakaho et al., 2004). We assume that the dynamics around a tipping point described here is a conserved trait of bacterial wilt, however its temporal positioning could vary depending on the plant species and plant age (which could influence immune response or root infection).

The plant water loss observed during *R. solanacearum* infection (Figure 3) is in a similar range to that observed during drought on tomato (Sánchez-Rodríguez et al., 2010), around 10% of water content, showing that bacterial wilt imposes significant drought stress on the plant. Photosynthesis requires a big amount of water, so water deficit should quickly impair photosynthesis and, therefore, have an impact on the ability to store carbon such as starch during the daytime phase of the day. In agreement with this, we observed in our metabolomic analysis a clear drop in starch storage in infected aerial parts at 7 dpi (Figure 3). The estimation of chlorophyll content by imaging revealed a progressive decrease after infection, which remained limited at 7 dpi (Figure 3). The incidence of bacterial wilt is probably less apparent on the chlorophyll content than on the accumulation of starch since chlorophyll,

even though described as decreasing under stress, is subjected to a turnover slower than starch (Scialdone et al., 2013).

Quantitative insights in *R. solanacearum* preferred carbon sources in xylem.

In a second part of this work, we studied the kinetic variations of metabolites of xylem sap associated with the bacterial wilt disease. The fast proliferation of *Ralstonia* spp in xylem must be sustained by nutrients that the pathogen uptakes in this environment. We therefore studied specifically the metabolites that were less abundant in the sap of infected plants compared to that of healthy plants, presumably used by bacteria for efficient growth. The PCA multivariate analysis of metabolomic data revealed that glutamine and asparagine are significantly depleted in infected plants. This is particularly striking for glutamine for which the initial concentration (2.66 ± 1.34 mM at 1 dpi) decreases to lower than 1 mM at the last days of sampling. Glutamine is described as the major organic component of xylem sap in plants of different botanical families (Andersen & Brodbeck, 1989; Montes Borrego, Miguel; Jiménez-Díaz et al., 2017; Zuluaga et al., 2013). Our data are in line with these reports: glutamine in tomato xylem sap was measured 3.29 ± 1.25 mM for non-infected plants, which represents 75% of the molar organic carbon in this compartment. We showed that glutamine concentration was negatively correlated with bacterial growth, supporting the view that glutamine is most probably the main carbon source sustaining fast proliferation in vascular tissues. As glutamine is by far the most abundant amino acid in xylem, we hypothesize that *R. solanacearum* has adapted to preferentially metabolize this compound. The five different transport systems for this compound present in the genome of GMI1000 highlight the high importance of this metabolite.

Simultaneously to glutamine, the asparagine pool (around 0.178 ± 0.074 mM in sap of healthy plants) is quickly depleted after 4 dpi, falling under the detection limit (between 1 µM and 10 µM). According to our data, sugars do not appear to play a major role as sources of energy supply for the bacteria in

xylem vessels. Indeed, sugars are present in scarce proportions compared to amino acids such as glutamine or asparagine. Glucose can be detected but in concentration at the limit of reliable detection, and the sucrose content also appears rather low. Thus, the sugars concentration does not seem sufficient to explain the strong bacterial growth. Bacterial infection should lead to the enrichment of the sap with sugars such as sucrose and glucose, as reported by (Lowe-Power, Hendrich, et al., 2018). However, based on the kinetic and quantitative values we hypothesized that these metabolites might have a role in signaling rather than being primary carbon sources to sustain rapid growth, unless sucrose/glucose dynamics is too fast to be captured by a day by day kinetics. This was confirmed by the behavior of a triple mutant strain that is unable to grow *in vitro* when glucose, sucrose and fructose are provided as sole carbon sources. This strain however is still able to colonize the plant, reaching high density in the stem, and causes physiological alteration in plants (suppression of growth and transpiration) and symptoms (disease index) delayed but similar to the wild-type strain. We thus concluded that sugars do not play a major role in the pathogen's growth at this stage.

Our metabolomics study also revealed that several potential nutrients (such as aspartate, phenylalanine and leucine) remain in xylem sap even at later infection stages in concentrations similar to that of healthy plants. This suggests that these metabolites are not consumed by *R. solanacearum*, probably due to the lack or non-expression of the appropriate transporter genes. For various other lower abundant nutrients, the high variability observed in infected plants prevents making clear conclusions. In an earlier study, Zuluaga et al. (2013) analyzed the xylem sap content of tomato and it should be noted that some carbon sources reported in their study were not detected in ours. This mainly concerns amino acids such as GABA (gamma-aminobutyric acid), histidine and serine. The presence of fructose was also detected while our data reveal the presence of sucrose but not fructose. Higher quantities of glucose, fructose and sucrose were found in the tomato apoplast (Zuluaga et al., 2013). However, as the GRS491 triple mutant strain was still able to cause effective bacterial wilt, this suggests that

metabolization of these sugars is also not essential for the growth of *R. solanacearum* in the apoplastic environment.

A recent study revealed glutamic acid as a major amino acid promoting expression of some *R. solanacearum* pathogenic traits (Shen et al. 2020) . Inversely to glutamine, glutamic acid is present in trace amounts in our xylem sap analysis (Table 1) and its concentration remains constant during infection. The NMR analysis of xylem sap unambiguously discriminated between the two amino acids (Fig. S10). Therefore, we favor a role of glutamic acid in signaling to induce production of virulence factors rather than as a major carbon source metabolized in xylem vessels.

Metabolic signatures of bacterial wilt.

Beside the depletion of some metabolites as mentioned above, we also observed the increase of other compounds in xylem following *R. solanacearum* infection. The emergence of such compounds could be from bacterial origin (excreted product such as putrescine (Lowe-Power, Hendrich, et al., 2018; Peyraud et al., 2016)), or part of a plant metabolic response to infection (Zeiss et al., 2019). In some cases, these compounds could come simultaneously from the bacteria and from the plant. In the case of putrescine, the role of the molecule may be dual since bacterial production has been shown to contribute to the wilt symptoms (Lowe-Power, Hendrich, et al., 2018) and also be produced by tomato cells hijacked by a *Ralstonia spp* TAL effector (Wu et al., 2019).

We found that upon infection xylem sap accumulated 3-hydroxybutyric acid, acetate, ethanol and potentially proline (discriminated by PCA, Figure 4 although no significant difference in the kinetics on Fig. S8). Accumulation of proline and ethanol has been associated with drought stress (Kelsey et al., 2014; Sánchez-Rodríguez et al., 2010) and one can assume that the bacterial wilt disease induces a sudden and brutal water deficit for the infected plant (Zeiss et al., 2019). Ethanol production could also be a physiological response to xylem occlusion by *R. solanacearum*: the formation of bacterial

biofilm would limit the diffusion of oxygen in the xylem vessels, thus inducing a switch to anaerobic respiration in plant cells and therefore the production of ethanol as a fermentation product. Concerning proline, its release into the xylem by plant cells may be due to the need to compensate for the depletion of glutamine / asparagine consumed by the bacteria. Acetate was also found to appear in infected xylem; similarly to ethanol, acetate could be a plant fermentation product due to a limitation of oxygen diffusion, but it could also result from an overflow of the bacterial metabolism (El-Mansi & Holms, 1989). As previously reported by Lowe-Power et al. (2018), we observed an increased synthesis of 3-hydroxybutryic acid. 3-hydroxybutyric acid is a precursor of PHB (polyhydroxybutyrate), a storage polymer identified in *R. solanacearum* and phylogenetically close β-proteobacteria. Kinetics showed an increase followed by a decrease phase of 3-hydroxybutyric acid concentration (Figure 4C), in agreement with the hypothesis that this metabolite could be excreted by *Ralstonia* and then consumed before returning to the soil (Lowe-Power et al., 2018). However, it cannot be excluded that bacteria induce production of 3-hydroxybutyric acid by the plant, as the biosynthetic pathway is present in tomato plant (Yuan et al., 2016).

In a complementary approach, Lowe-Power and collaborators (2018) have recently performed GC-MS metabolomics of tomato xylem sap infected by *R. solanacearum*. This allowed a non-targeted approach but not an absolute quantification of the metabolites as we were able to achieve it by the NMR approach. Based on the relative fold-change of metabolites in the xylem sap of healthy versus infected plants, several carbon sources such as galactose, 3-hydroxybutyrate, gluconate and glucose were identified as important carbon sources for *R. solanacearum* in the xylem (Lowe-Power, Hendrich, et al., 2018). In our study, except for 3-hydroxybutyric acid and glucose (at a concentration below 0.1 mM), the other compounds were not detected, indicating that these compounds are in concentration below 1 – 10 µM, which is the sensibility limit of NMR. Significant change folds can be observed more easily for low-concentration metabolites than for abundant ones. This thus suggests that the metabolites, even if they had high fold change, are probably not primary carbon sources supporting

bacterial growth. Given the quantities of carbon source available in tomato xylem sap and their observed consumption by *R. solanacearum* (Figure 5), the most likely hypothesis is that co-consumption of glutamine and asparagine is the main means used by the pathogen to support its high proliferation in xylem. The redundancy observed in the genome at the level of glutamine transporter genes (five unlinked loci identified) reinforces the view that this amino acid is probably crucial to the *R. solanacearum* fitness inside the plant vascular system.

Experimental procedures

Plant cultures and automatic phenotyping

Two independent experiments were conducted for this study. In both cases, tomato seeds (*Solanum lycopersicum* M82) were grown in soil (SB2, Proveen, The Netherlands) supplemented with Osmocote® coated fertilizer at a rate of 4g/L. Seed were germinated in a growth chamber (26°C, 67% HR, 12h- LED light per day). Around a hundred of plantlets were transplanted in individual plastic pots (8x8cm) 8 days after sowing. 16 days after sowing, 90 young plants were chosen and repotted in 3L pots until the end of the experiment. Foam cover discs were placed on each pot to limit the evaporation.

On the first experiment, 90 plants were loaded on the Phenoserre robot facility of the Toulouse Plant Microbe Phenotyping infrastructure, of which 45 plants were inoculated with *R. pseudosolanacearum* GMI1000 strain (Salanoubat et al., 2002) and another 45 mock-inoculated with sterile water (referred to as “Healthy plants”). 12h-light per day at 28°C and 50% humidity were programmed. On the second experiment, 81 plants were loaded on the Phenoserre robot, of which 63 infected and 18 healthy plants.

All the plants were watered with 100 ml three times on the loading day and weighted, in order to define a well-watered target weight. The subsequent watering was conducted automatically once a day to the target weight. Imaging was programmed four times a day (starts at 2.00 a.m., 9.00 a.m., 4.30 p.m, and 7.30 p.m, for a total duration of around one hour and a half per imaging job), the conveyor belt bringing the individual plants to a side-RGB camera. The plants were then automatically weighted after each imaging session. The daily transpiration was determined as the weight differences between two consecutive days, at the time of watering. Temperature, hygrometry and light intensity were recorded during the whole experiment.

Plant image analysis

Fig. S1 presents the step-by-step segmentation performed using a set of python algorithms allowing for the testing of the segmentation pipeline. Every plant is imaged using an RGB camera with a blue background, under six angles (stating at 0° and then by 60° steps). Three different "Region of Interest" or ROIs are defined to allow easier analysis, in white containing all the plant information, with a "safe zone" in green and a "danger zone" in red. As the images are acquired in the exact same conditions, the ROIs are static. Masks are extracted corresponding to the bulk of the plant ("mask top"), as well as two additional masks to gather the plant information close to the pot and conveyor ("mask middle" and "mask bottom"). All three masks are merged in order to build a coarse mask, this latter ask is then cleaned by removed additional noise to generate a clean mask and allowing for the final features extraction.

Fig S2, displays the "centroid y" (or Cy) morphological traits, which is the y coordinate of the plant area center of gravity. The origin of the y axe is positioned at the top of the image. A larger Cy value indicates a center of gravity closer to the pot (further from the top of the image) and is a trait that is very well associated with the bacterial wilt symptoms, as any "lowering" of the leaves (wilting) has an impact of the Cy trait. Fig S3 displays some Cy values of plants with different disease index (DI).

Plant inoculation

For both experiments, three replicates of the strain GMI1000 were grown in BG complete medium (Plener et al., 2010) at 28°C. Bacterial cells were washed, resuspended in sterile water and each plant was inoculated with one of the three replicates by pouring 50 ml of a suspension at $5 \cdot 10^6$ CFU/ml at the stem base 4 days after the loading on the robot. Just before inoculation, roots were scarified with a scalpel blade in order to synchronize the infection rate.

Collection and preparation of plant samples

For the first experiment, plants were removed each day from the conveyor belt for samplings during 9 consecutive days. On the inoculation day and at 7 and 8 dpi, 3 healthy and 3 infected plants were

475 removed. From 2 to 6 dpi, 6 healthy and 6 infected plants were removed each day. For the second
476 experiment, plants were removed from the conveyor belts for samplings at 1, 3, 4, 5, 7 and 8 dpi. Each
477 sampling day, 3 healthy plants and respectively, 3, 6, 14, 16, 14, 10 infected plant were removed.

478 In both experiments, the following procedures were then applied at the same period of the day (between
479 10 am and 2 pm) to avoid the effect of daily variations in xylem sap/organ chemistry. For the plant
480 that were removed from the experimental setup, stems were cut just above the cotyledon node, rinsed
481 with approximately 1 ml of water and the upcoming xylem sap was collected by repeated pipetting
482 and collection in Eppendorf tubes placed on ice. For the infected plants, the tubes were centrifuged
483 and the supernatants were transferred in new tubes while the pellets were discarded. The tubes with
484 xylem sap were placed at -80°C for further quantitative NMR analyses.

485 The different organs of each plant were collected separately (stems, leaves, roots and flowers whenever
486 they occurred) for fresh and dry weights measurements. Approximately 300 mg fresh weight for each
487 collected organ was frozen in liquid nitrogen and stored at -20°C for further biochemical analyses.

488 1 cm of stem was sampled above the cotyledons, cut up in small pieces and placed in a 2 ml centrifuge
489 tube containing glass beads (2 mm diameter) and ground at 30 Hz with a mixer mill (MM 400, Retsch,
490 Germany) until total grinding (1 to 3 minutes). Extracted bacteria were resuspended in 1 ml of sterile
491 water, serial-diluted and plated on complete BG medium supplemented with triphenyl tetrazolium
492 chloride, for counting as previously described (Guidot et al., 2014).

493

494 **Quantitative NMR analyses**

495 The xylem saps were analyzed by 1D ^{1}H NMR on MetaToul analytics platform (UMR5504, UMR792,
496 CNRS, INRAE, INSA 135 Avenue de Rangueil 31077 Toulouse Cedex 04, France), using the Bruker
497 Avance 800 MHz equipped with an ATMA 5mm cryoprobe. Each xylem sap sample was centrifuged
498 to remove the residues (5min, 13520 RCF, Hettich Mikro 200 centrifuge), then placed in 3 mm NMR

tubes. TSP-d4 standard (Sodium 3-(trimethylsilyl)(1-13C,2H4)propanoate), at a final concentration of 100 µM, was used as a reference. pH 6.0 phosphate buffer was used to standardize the chemical shifts among samples. Acquisition conditions were as follows: 30° pulse angle, 20.0287 ppm spectral width, 64 scans per acquisition for a total scan time of approximately 8 minutes per sample, and zgpr30 water pre-saturation sequence. The samples were kept at a temperature of 280 K (6.85 °C) all along the analysis. Resonances of metabolites were manually integrated and the concentrations were calculated based on the number of equivalent protons for each integrated signal and on the TSP final concentration. For one equivalent proton, half of the glucose signal was overlapped by the residual water, as shown on Fig. S10 (around 5.2 ppm). Therefore, its contribution was extrapolated based on the analysis of a glucose standard.

Biochemical analyses of metabolites

Quantifications of metabolites were performed at the HitMe platform (INRAE - IBVM - 71 avenue E. Bourlaux - CS 20032 - 33882 Villenave d'Ornon Cedex, France). The plants samples, previously frozen in liquid nitrogen, were ground to a powder using liquid nitrogen to avoid thawing. A quantity of 20 +/- 10 mg of each were weighted in previously frozen Micronic tubes. Free amino acids, glucose, fructose, malate, proteins, starch, sucrose and chlorophylls in leaves, stems and roots were quantified as described in (Biais et al., 2014). Briefly, ethanolic extracts from every samples were obtained using three consecutive incubation of the frozen ground powder aliquots. Ethanol 80% v/v with HEPES/KOH 10 mM pH6 buffer was used for the two first incubations, and ethanol 50% v/v with HEPES/KOH 10 mM pH6 buffer was used for the third. Supernatants were pooled and used for the quantification of chlorophylls, glucose, fructose, sucrose, malate and free amino acids. Pellets were used for the determination of protein and starch contents. The extracts and pellets were stored at -20°C between each quantification. For each sample, chlorophylls were quantified by measuring optical densities at 645 and 665 nm on a mix of 50 µl of extract supplemented with 150 µl of analytics grade

ethanol. Amino acids were quantified using the fluorescamine method. Excitation wavelength was 405nm and emission was measured at 485 nm. The proteins were quantified using Bradford reagent. Starch was quantified in glucose equivalent after full pellet digestion in an oven at 37°C for 18 hours. For the other analytes cited above, the NADH/NADPH appearance was measured, and the analytes were quantified using a 1:1 stoichiometric coefficient.

Generation and phenotyping of *R. solanacearum* triple mutant strain defective for glucose, sucrose and fructose assimilation

Strain GRS941 was engineered by cumulating deletions in the glucose transport operon (RSp1632-RSp1635), the sucrose assimilation operon (RSp1280-RSp1286) and the fructose transport operon (RSc2861-RSc2863). Complete procedures for the triple mutant generation are available on Text S1. For *in vitro* growth assay, preculture on BG complete medium (Plener et al., 2010), cell centrifugation/washing and resuspension were performed. Strains were then inoculated at an OD (600 nm) of 0.01 on minimal medium (Plener et al., 2010) supplemented with respectively glucose, sucrose, fructose, glutamine as sole carbon source (at 50 mM of carbon). Growth was assessed using microplate spectrophotometer (FLUOstar Omega, BMG Labtech, Germany) during 96h at 28°C and under shaking at 700 rpm. For in planta phenotyping, the same procedure than described for the GMI1000 strain was followed on two independent experiments, with respectively 31 and 41 tomato plants infected by the mutant strain and similar number of plants infected by the wild-type strain..

Supporting Information

Acknowledgments

LG was funded by a PhD grant from the French Ministry of National Education and Research. AE was funded by the French Laboratory of Excellence TULIP (ANR-10-LABX-41 and ANR-11-IDEX-0002-02). The study was funded by the French Laboratory of Excellence (LABEX) project TULIP (ANR-10-LABX-41 and ANR-11-IDEX-0002-02). The funders had no role in study design, data collection and analysis, decision to publish, or preparation of the manuscript.

We thank TPMP (Toulouse Plant Microbe Phenotyping) platform (Castanet-Tolosan, France) and its staff Fabrice Devoilles for their technical support in plant cultures and imaging, as well as HiTMe (High-Throughput Metabolic phenotyping) platform (Villenave d'Ornon, France) for biochemical analysis of organ metabolites. We acknowledge MetaToul (Metabolomics & Fluxomics Facitilies, Toulouse, France, www.metatoul.fr) platform, which is part of the MetaboHUB-ANR-11-INBS-0010 national infrastructure (www.metabohub.fr) and its staff Cécilia Berges, Edern Cahoreau and Lindsay Peyriga for access to NMR facilities. We also thank Patrick Barberis for his expert skills in the construction of the triple mutant strain.

Author contributions

Conceptualization: SG, CB. Methodology: LG, AE, NP, SG, CB. Formal analysis: LG, AE, FMM, CB. Investigation: LG, AE, CC, CB. Resources: NP. Writing – Original Draft: LG, AE. Writing – Review & Editing: LG, AE, NP, SG, CB. Visualization: LG, AE. Project administration: CB. Funding acquisition: CB.

Data availability statement

All data supporting the findings of this study are available within the paper and within its supplementary materials published online.

Conflict of interests. The authors declare no competing interests.

References

Álvarez, B., Biosca, E. G., & López, M. M. (2010). On the life of Ralstonia solanacearum, a destructive bacterial plant pathogen. *Current Research, Technology and Education Topics in Applied Microbiology and Microbial Biotechnology*, 267–279. https://pdfs.semanticscholar.org/aa85/77e213e2977a0e4eb739795e3fea51187181.pdf?_ga=2.156465595.1055873898.1504096691-1311319012.1504096691

Andersen, P. C., & Brodbeck, B. V. (1989). Diurnal and temporal changes in the chemical profile of xylem exudate from Vitis rotundifolia. *Physiologia Plantarum*, *75*(1), 63–70. https://doi.org/10.1111/j.1399-3054.1989.tb02064.x

Angot, A., Peeters, N., Lechner, E., Vailleau, F., Baud, C., Gentzbittel, L., Sartorel, E., Genschik, P., Boucher, C., & Genin, S. (2006). Ralstonia solanacearum requires F-box-like domain-containing type III effectors to promote disease on several host plants. *Proceedings of the National Academy of Sciences of the United States of America*, *103*(39), 14620–14625. https://doi.org/10.1073/pnas.0509393103

Arlat, M., & Boucher, C. (1991). Research Notes Identification of a dsp DNA Region Controlling Aggressiveness of Pseudomonas solanacearum. *Molecular Plant-Microbe Interactions*, *4*(2), 211. https://doi.org/10.1094/mpmi-4-211

Biais, B., Bénard, C., Beauvoit, B., Colombié, S., Prodhomme, D., Ménard, G., Bernillon, S., Gehl, B., Gautier, H., Ballias, P., Mazat, J. P., Sweetlove, L., Génard, M., & Gibon, Y. (2014). Remarkable reproducibility of enzyme activity profiles in tomato fruits grown under contrasting environments provides a roadmap for studies of fruitmetabolism. *Plant Physiology*, *164*(3), 1204–1221. https://doi.org/10.1104/pp.113.231241

Caldwell, D., Kim, B.-S., & Iyer-Pascuzzi, A. S. (2017). *Ralstonia solanacearum* Differentially

611 Colonizes Roots of Resistant and Susceptible Tomato Plants. *Phytopathology*, *107*(5), 528–536.
612 https://doi.org/10.1094/PHYTO-09-16-0353-R

613 El-Mansi, E. M. T., & Holms, W. H. (1989). Control of carbon flux to acetate excretion during
614 growth of Escherichia coli in batch and continuous cultures. *Journal of General Microbiology*,
615 *135*(11), 2875–2883. https://doi.org/10.1099/00221287-135-11-2875

616 Fegan, M., & Prior, P. (2005). How complex is the "Ralstonia solanacearum species complex"?
617 *Bacterial Wilt Disease and the Ralstonia Solanacearum Species Complex*, *July*, 449–461.

618 Genin, S., & Denny, T. P. (2012). Pathogenomics of the *Ralstonia solanacearum* Species Complex.
619 *Annual Review of Phytopathology*, *50*(1), 67–89. https://doi.org/10.1146/annurev-phyto-
620 081211-173000

621 Guidot, A., Jiang, W., Ferdy, J. B., Thébaud, C., Barberis, P., Gouzy, J., & Genin, S. (2014).
622 Multihost experimental evolution of the pathogen ralstonia solanacearum unveils genes
623 involved in adaptation to plants. *Molecular Biology and Evolution*, *31*(11), 2913–2928.
624 https://doi.org/10.1093/molbev/msu229

625 Hamilton, C. D., Steidl, O. R., MacIntyre, A. M., Hendrich, C. G., & Allen, C. (2021). Ralstonia
626 solanacearum depends on catabolism of myo-inositol, sucrose, and trehalose for virulence in an
627 infection stage-dependent manner. *Molecular Plant-Microbe Interactions®*, MPMI-10-20-
628 0298-R. https://doi.org/10.1094/MPMI-10-20-0298-R

629 Hayward, A. C. (1991). Biology and Epidemiology of Bacterial Wilt Caused by Pseudomonas
630 Solanacearum. *Annual Review of Phytopathology*, *29*(1), 65–87.
631 https://doi.org/10.1146/annurev.py.29.090191.000433

632 Hikichi, Y., Mori, Y., Ishikawa, S., Hayashi, K., Ohnishi, K., Kiba, A., & Kai, K. (2017). Regulation
633 Involved in Colonization of Intercellular Spaces of Host Plants in Ralstonia solanacearum.

Frontiers in Plant Science, *8*, 967. https://doi.org/10.3389/fpls.2017.00967

Kelsey, R. G., Gallego, D., Sánchez-García, F. J., & Pajares, J. A. (2014). Ethanol accumulation during severe drought may signal tree vulnerability to detection and attack by bark beetles. *Canadian Journal of Forest Research*, *44*(6), 554–561. https://doi.org/10.1139/cjfr-2013-0428

Khokhani, D., Lowe-Power, T. M., Tran, T. M., & Allen, C. (2017). A Single Regulator Mediates Strategic Switching between Attachment/Spread and Growth/Virulence in the Plant Pathogen Ralstonia solanacearum. *MBio*, *8*(5), e00895-17. https://doi.org/10.1128/mBio.00895-17

Landry, D., González-Fuente, M., Deslandes, L., & Peeters, N. (2020). The large, diverse, and robust arsenal of Ralstonia solanacearum type III effectors and their in planta functions. *Molecular Plant Pathology*, *April*, 1–12. https://doi.org/10.1111/mpp.12977

Lebeau, A., Daunay, M. C., Frary, A., Palloix, A., Wang, J. F., Dintinger, J., Chiroleu, F., Wicker, E., & Prior, P. (2011). Bacterial wilt resistance in tomato, pepper, and eggplant: Genetic resources respond to diverse strains in the Ralstonia solanacearum species complex. *Phytopathology*, *101*(1), 154–165. https://doi.org/10.1094/PHYTO-02-10-0048

Liang, Y., Urano, D., Liao, K. L., Hedrick, T. L., Gao, Y., & Jones, A. M. (2017). A nondestructive method to estimate the chlorophyll content of Arabidopsis seedlings. *Plant Methods*, *13*(1), 26. https://doi.org/10.1186/s13007-017-0174-6

Lowe-Power, T. M., Hendrich, C. G., von Roepenack-Lahaye, E., Li, B., Wu, D., Mitra, R., Dalsing, B. L., Ricca, P., Naidoo, J., Cook, D., Jancewicz, A., Masson, P., Thomma, B., Lahaye, T., Michael, A. J., & Allen, C. (2018). Metabolomics of tomato xylem sap during bacterial wilt reveals *Ralstonia solanacearum* produces abundant putrescine, a metabolite that accelerates wilt disease. *Environmental Microbiology*, *20*(4), 1330–1349. https://doi.org/10.1111/1462-2920.14020

657 Lowe-Power, T. M., Khokhani, D., & Allen, C. (2018). How Ralstonia solanacearum Exploits and
658 Thrives in the Flowing Plant Xylem Environment. *Trends in Microbiology*, *26*(11), 929–942.
659 https://doi.org/10.1016/j.tim.2018.06.002

660 Montes Borrego, Miguel; Jiménez-Díaz, R. M. ;, Trapero Casas, J. L. ;, Navas Cortés, Juan Antonio ;
661 Haro, C., Rivas, J. C. ., Fuente, L. de la;, & Landa, B. B. (2017). Metabolomic characterization
662 of xylem sap of different olive cultivars growing in Spain. *European Conference on Xylella*,
663 *November*.

664 Morel, A., Guinard, J., Lonjon, F., Sujeeun, L., Barberis, P., Genin, S., Vailleau, F., Daunay, M. C.,
665 Dintinger, J., Poussier, S., Peeters, N., & Wicker, E. (2018). The eggplant AG91-25 recognizes
666 the Type III-secreted effector RipAX2 to trigger resistance to bacterial wilt (Ralstonia
667 solanacearum species complex). *Molecular Plant Pathology*, *19*(11), 2459–2472.
668 https://doi.org/10.1111/mpp.12724

669 Morel, A., Peeters, N., Vailleau, F., Barberis, P., Jiang, G., Berthomé, R., & Guidot, A. (2018). Plant
670 pathogenicity phenotyping of Ralstonia solanacearum strains. In *Methods in Molecular Biology*
671 (Vol. 1734, pp. 223–239). Humana Press Inc. https://doi.org/10.1007/978-1-4939-7604-1_18

672 Nakaho, K., Inoue, H., Takayama, T., & Miyagawa, H. (2004). Distribution and multiplication of
673 Ralstonia solanacearum in tomato plants with resistance derived from different origins. *Journal*
674 *of General Plant Pathology*, *70*(2), 115–119. https://doi.org/10.1007/s10327-003-0097-0

675 Perrier, A., Barlet, X., Rengel, D., Prior, P., Poussier, S., Genin, S., & Guidot, A. (2019).
676 Spontaneous mutations in a regulatory gene induce phenotypic heterogeneity and adaptation of
677 Ralstonia solanacearum to changing environments. *Environmental Microbiology*, *21*(8), 3140–
678 3152. https://doi.org/10.1111/1462-2920.14717

679 Peyraud, R., Cottret, L., Marmiesse, L., & Genin, S. (2018). Control of primary metabolism by a
680 virulence regulatory network promotes robustness in a plant pathogen. *Nature Communications*,

681 *9*(1), 418. https://doi.org/10.1038/s41467-017-02660-4

682 Peyraud, R., Cottret, L., Marmiesse, L., Gouzy, J., & Genin, S. (2016). A Resource Allocation
683 Trade-Off between Virulence and Proliferation Drives Metabolic Versatility in the Plant
684 Pathogen Ralstonia solanacearum. *PLoS Pathogens*, *12*(10), e1005939.
685 https://doi.org/10.1371/journal.ppat.1005939

686 Planas-Marquès, M., Kressin, J. P., Kashyap, A., Panthee, D. R., Louws, F. J., Coll, N. S., & Valls,
687 M. (2020). Four bottlenecks restrict colonization and invasion by the pathogen Ralstonia
688 solanacearum in resistant tomato. *Journal of Experimental Botany*, *71*(6), 2157–2171.
689 https://doi.org/10.1093/jxb/erz562

690 Plener, L., Manfredi, P., Valls, M., & Genin, S. (2010). PrhG, a transcriptional regulator responding
691 to growth conditions, is involved in the control of the type III secretion system regulon in
692 Ralstonia solanacearum. *Journal of Bacteriology*, *192*(4), 1011–1019.
693 https://doi.org/10.1128/JB.01189-09

694 Poueymiro, M., Cunnac, S., Barberis, P., Deslandes, L., Peeters, N., Cazale-Noel, A. C., Boucher, C.,
695 & Genin, S. (2009). Two type III secretion system effectors from Ralstonia solanacearum
696 GMI1000 determine host-range Specificity on Tobacco. *Molecular Plant-Microbe Interactions*,
697 *22*(5), 538–550. https://doi.org/10.1094/MPMI-22-5-0538

698 Prior, P., Ailloud, F., Dalsing, B. L., Remenant, B., Sanchez, B., & Allen, C. (2016). Genomic and
699 proteomic evidence supporting the division of the plant pathogen Ralstonia solanacearum into
700 three species. *BMC Genomics*, *17*(1), 1–11. https://doi.org/10.1186/s12864-016-2413-z

701 Safni, I., Cleenwerck, I., De Vos, P., Fegan, M., Sly, L., & Kappler, U. (2014). Polyphasic
702 taxonomic revision of the Ralstonia solanacearum species complex: Proposal to emend the
703 descriptions of Ralstonia solanacearum and Ralstonia syzygii and reclassify current R. syzygii
704 strains as Ralstonia syzygii subsp. syzygii subsp. nov., R. s. *International Journal of Systematic*

and Evolutionary Microbiology, *64*, 3087–3103. https://doi.org/10.1099/ijs.0.066712-0

Salanoubat, M., Genin, S., Artiguenave, F., Gouzy, J., Mangenot, S., Arlat, M., Billault, A., Brottiert, P., Camus, J. C., Cattolico, L., Chandler, M., Choisne, N., Claudel-Renard, C., Cunnac, S., Demange, N., Gaspin, C., Lavie, M., Moisan, A., Robert, C., … Boucher, C. A. (2002). Genome sequence of the plant pathogen Ralstonia solanacearum. *Nature*, *415*(6871), 497–502. https://doi.org/10.1038/415497a

Sánchez-Rodríguez, E., Rubio-Wilhelmi, Mm., Cervilla, L. M., Blasco, B., Rios, J. J., Rosales, M. A., Romero, L., & Ruiz, J. M. (2010). Genotypic differences in some physiological parameters symptomatic for oxidative stress under moderate drought in tomato plants. *Plant Science*, *178*(1), 30–40. https://doi.org/10.1016/j.plantsci.2009.10.001

Scialdone, A., Mugford, S. T., Feike, D., Skeffngton, A., Borrill, P., Graf, A., Smith, A. M., & Howard, M. (2013). Arabidopsis plants perform arithmetic division to prevent starvation at night. *ELife*, *2013*(2). https://doi.org/10.7554/eLife.00669

Shen, F., Yin, W., Song, S., Zhang, Z., Ye, P., Zhang, Y., Zhou, J., He, F., Li, P., & Deng, Y. (2020). *Ralstonia solanacearum* promotes pathogenicity by utilizing <scp>l</scp> -glutamic acid from host plants. *Molecular Plant Pathology*, *21*(8), 1099–1110. https://doi.org/10.1111/mpp.12963

Vasse, J., Frey, P., & Trigalet, A. (1995). Microscopic studies of intercellular infection and protoxylem invasion of tomato roots by Pseudomonas solanacearum. *Molecular Plant-Microbe Interactions*, *8*(2), 241–251. https://doi.org/10.1094/MPMI-8-0241

Wu, D., von Roepenack-Lahaye, E., Buntru, M., de Lange, O., Schandry, N., Pérez-Quintero, A. L., Weinberg, Z., Lowe-Power, T. M., Szurek, B., Michael, A. J., Allen, C., Schillberg, S., & Lahaye, T. (2019). A Plant Pathogen Type III Effector Protein Subverts Translational Regulation to Boost Host Polyamine Levels. *Cell Host and Microbe*, *26*(5), 638-649.e5. https://doi.org/10.1016/j.chom.2019.09.014

729 Xue, H., Lozano-Durán, R., & Macho, A. P. (2020). Insights into the Root Invasion by the Plant
730 Pathogenic Bacterium Ralstonia solanacearum. *Plants*, *9*(4), 516.
731 https://doi.org/10.3390/plants9040516

732 Yuan, H., Cheung, C. Y. M., Poolman, M. G., Hilbers, P. A. J., & van Riel, N. A. W. (2016). A
733 genome-scale metabolic network reconstruction of tomato (Solanum lycopersicum L.) and its
734 application to photorespiratory metabolism. *The Plant Journal : For Cell and Molecular*
735 *Biology*, *85*(2), 289–304. https://doi.org/10.1111/tpj.13075

736 Zeiss, D. R., Mhlongo, M. I., Tugizimana, F., Steenkamp, P. A., & Dubery, I. A. (2019).
737 Metabolomic Profiling of the Host Response of Tomato (Solanum lycopersicum) Following
738 Infection by Ralstonia solanacearum. *International Journal of Molecular Sciences 2019, Vol.*
739 *20, Page 3945*, *20*(16), 3945. https://doi.org/10.3390/IJMS20163945

740 Zuluaga, A. P., Puigvert, M., & Valls, M. (2013). Novel plant inputs influencing Ralstonia
741 solanacearum during infection. *Frontiers in Microbiology*, *4*(NOV), 349.
742 https://doi.org/10.3389/fmicb.2013.00349

743

744

745 **Figure and table legends**

746 **Table 1. Xylem metabolite content and the impact of *R. solanacearum* infection**

747 1: Effect of infection was deduced from the PCA presented in Figure 4. Metabolite concentration
748 decrease was assigned for compounds with loading weights on the second component inferior to -0.3
749 whereas increase in concentration was assigned for those superior to 0.3. Values ranging between -
750 0.15 and -0.3 correspond to compounds with putative decrease in concentration, those between 0.15
751 and 0.3 to putative increase. Values ranging from -0.15 and 0.15 defined compounds with no
752 significant variation in concentration (ie not impacted by infection). Putrescine was considered as
753 'appearing' as it was absent in healthy plants and had a loading weight on the second component
754 superior to 0.3. (see Table S2)

755 2: Usage as carbon source (+: growth, -: no growth) was assessed from published Biolog Phenotype
756 Microarrays data (Peyraud et al., 2016).

757 **Figure 1**

758 Impact of *R. solanacearum* colonization on plant physiology (dry weight/transpiration) and monitoring
759 of disease kinetics (disease index/bacterial density). The data presented are from an experiment on 81
760 plants, with at least 3 plants per conditions at each sampling point. Bars indicate standard deviation.
761 Healthy and infected plant data (transpiration and dry weight) were compared by Wilcoxon-Mann-
762 Whitney test (*: p-value<0.05, **: p-value<0.01, ****: p-value <0.0001).

763 **Figure 2**

764 Physiological parameters determined by automatic imaging. Chlorophyll content was estimated
765 through RGB values of plant images as described by Liang et al *(Liang et al., 2017)*. Center of
766 gravity position (vertical) was estimated through plant imaging with 0 pixel representing the top of
767 the plant. The data presented are from an experiment on 81 plants with at least 3 plants per
768 conditions at each sampling point. Bars indicate standard deviation. Healthy and infected plant data

were compared by Wilcoxon-Mann-Whitney test (*: p-value<0.05, **: p-value<0.01, ****: p-value <0.0001).

Figure 3

Impact of *R. solanacearum* infection on plant tissues. A. Tissue hydration. Fresh weight and dry weight were used to determine the proportion of water in healthy and infected tissues. Bars indicate standard deviation. B. Metabolic profile of tissues expressed in percentage of dry weight for starch and amino acids. The mean and standard deviation displayed were obtained after combining the acquired data of the two biological replicates (total of 12 samples for leaf, 10 for stem, 12 for root at each time point). In A. and B., healthy and infected plant data were compared by Wilcoxon-Mann-Whitney test (*: p-value<0.05, **: p-value<0.01).

Figure 4

Principal Component Analysis on metabolite concentrations from samples at different dpi. Representation of individual points (A) and the variables (B). Zero bacterial population corresponds to healthy plant samples. Data points at the top of the plot correspond to uninfected or low bacterial population samples while data points at the bottom correspond to high bacterial population samples. Principal component 1: 35% of variability. Principal component 2: 27% of variability. ETOH: ethanol, PUTR: putrescine, FUM: fumarate, SUC: sucrose, GLC: glucose.

Figure 5

Kinetics of metabolic contents in xylem sap of infected or healthy plants based on a total of 57 xylem sap samples obtained at different dpi. Healthy and infected plant data were compared by Wilcoxon-Mann-Whitney test (*: p-value<0.05, **: p-value<0.01).

Figure 6

Correlations between markers of the infection. For CFU per g of fresh weight, only data for which the counting was above 10^7 CFU per of fresh weight (corresponding to the “tipping point”) were included.

Figure 7

In vitro and in planta behavior of the *R. solanacearum* mutant strain GRS941 (carrying deletion in the sucrose, glucose and fructose transporter genes), compared to the wild-type strain GMI1000. Growth on minimal medium supplemented with sucrose (A) and glucose (B) as sole carbon source monitored in microplates with three independent biological replicates. Means and standard deviations are represented by the lines and colored areas, respectively. Bacterial density in planta (C) was determined on at least 9 plants per condition and per day, and plant transpiration (D) on at least 7 plants per condition and per day for infected WT/GRS941 (except 3 at 8 dpi) and at least 3 plants per day for healthy plants. Means are presented and bars indicate standard-deviation.

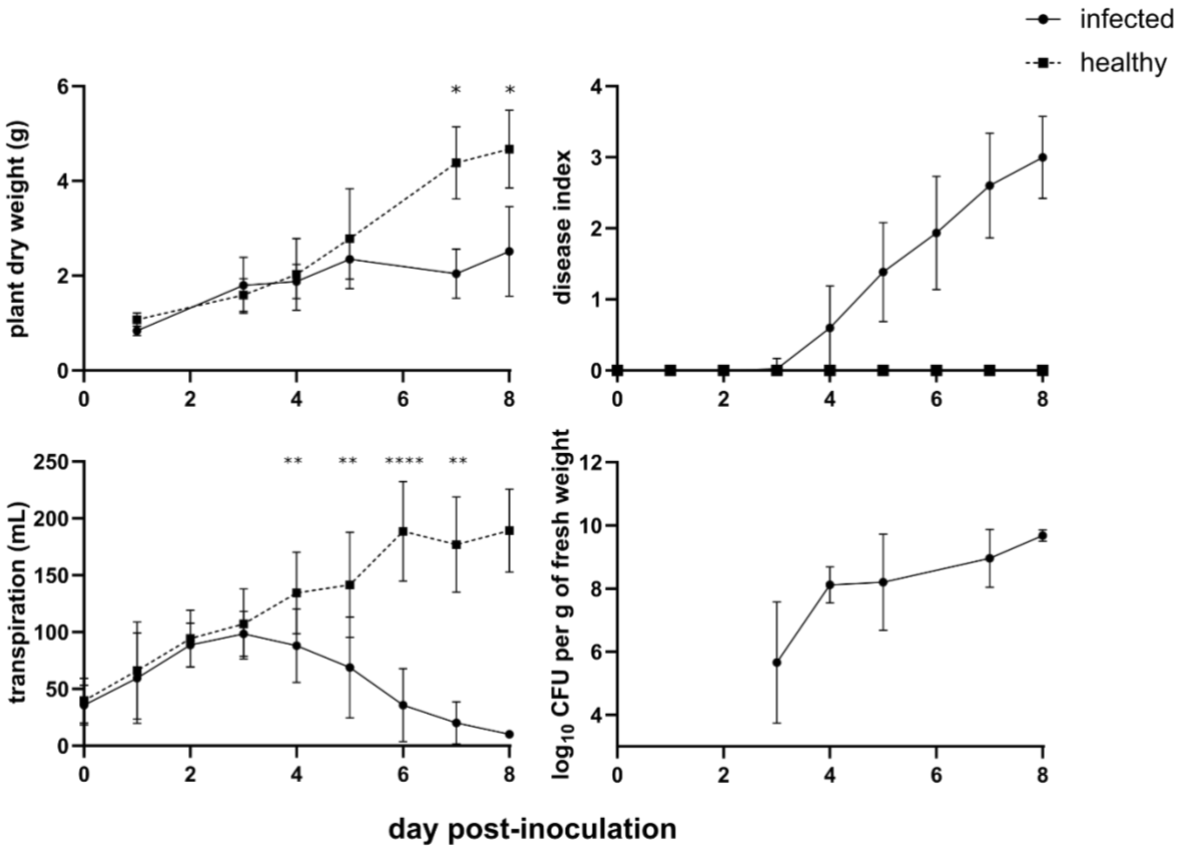
infected
healthy
plant dry weight (g)
disease index
transpiration (mL)
log10 CFU per g of fresh weight
day post-inoculation
*
*
**
**
****
**

Figure 1

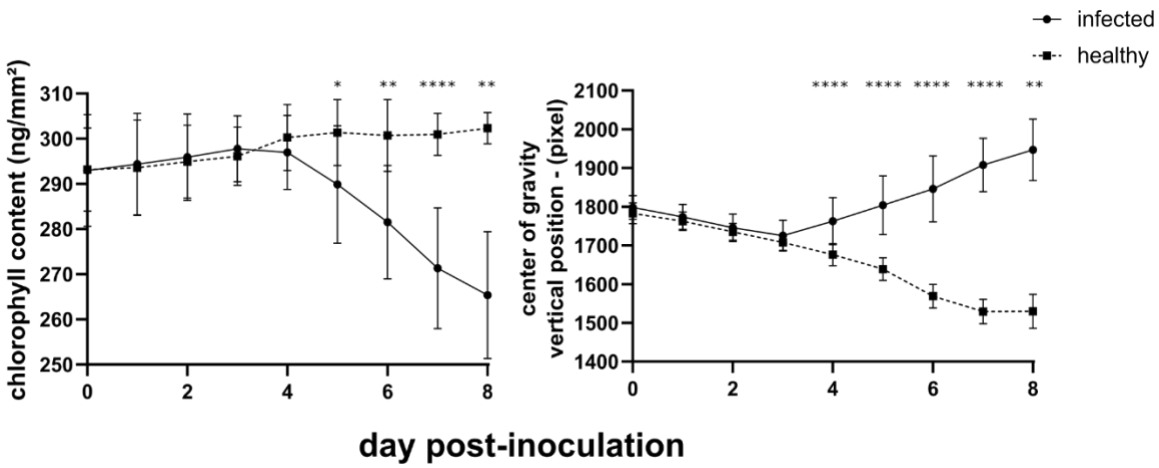
infected
healthy
chlorophyll content (ng/mm²)
center of gravity
vertical position - (pixel)
day post-inoculation

Figure 2

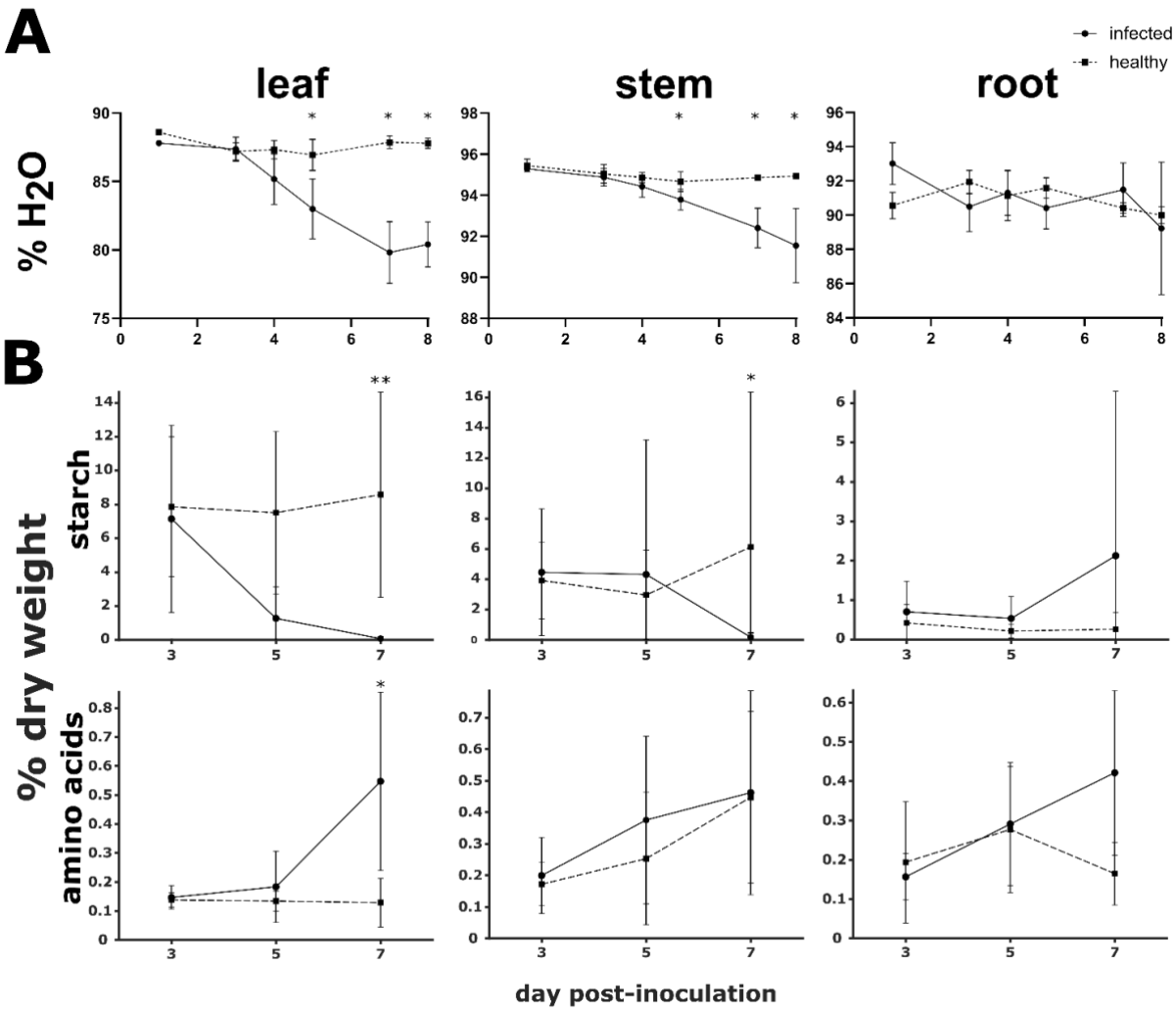
A
leaf
stem
root
infected
healthy
% H2O
B
% dry weight
starch
amino acids
day post-inoculation

Figure 3

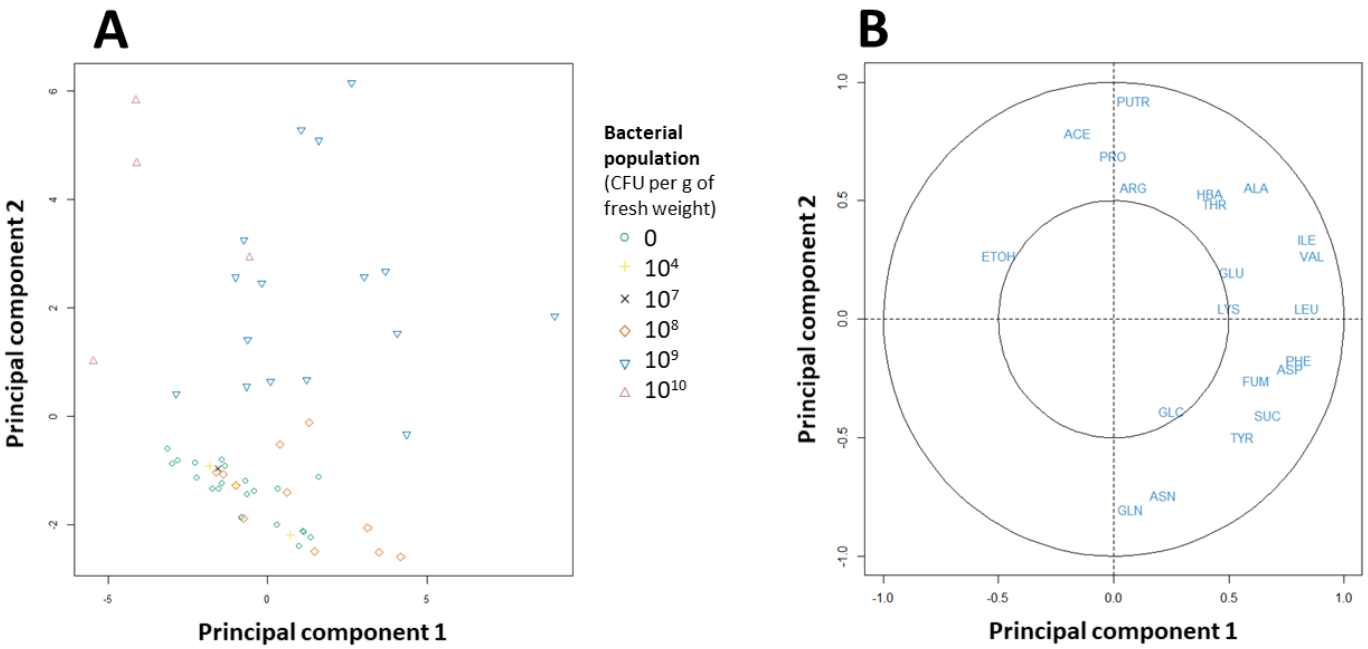
A
Principal component 2
Principal component 1
Bacterial population
(CFU per g of fresh weight)
0
10^4
10^7
10^8
10^9
10^10
B
Principal component 2
Principal component 1
PUTR
ACE
PRO
ARG
HBA
THR
ALA
ILE
VAL
ETOH
GLU
LYS
LEU
PHE
ASP
FUM
GLC
SUC
TYR
ASN
GLN

Figure 4

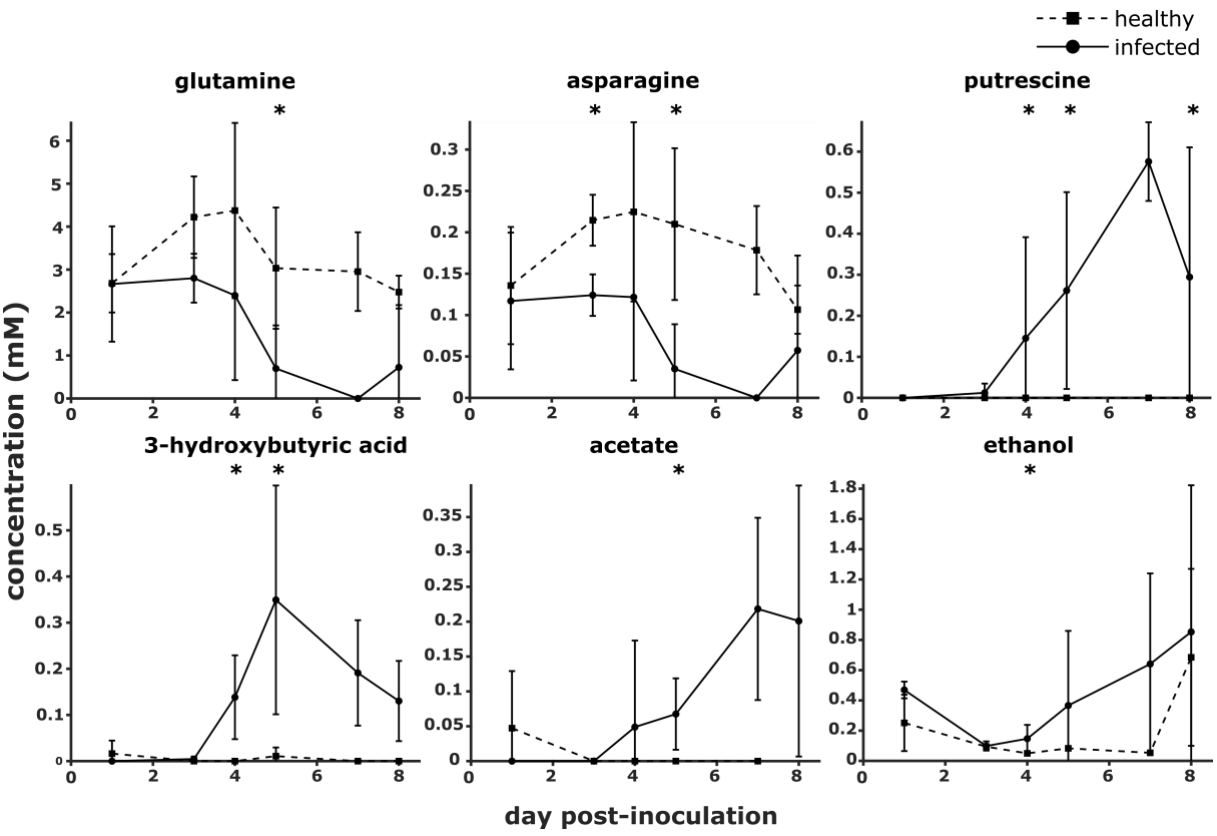
healthy
infected
glutamine
asparagine
putrescine
3-hydroxybutyric acid
acetate
ethanol
concentration (mM)
day post-inoculation

Figure 5

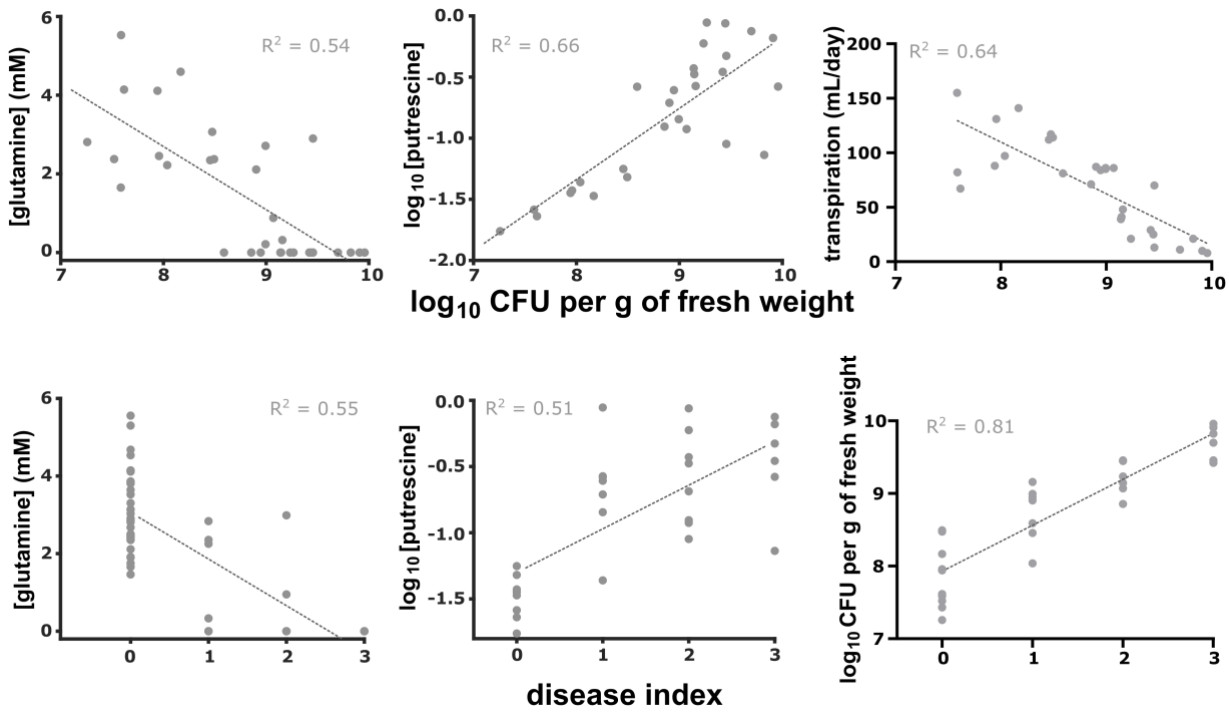
[glutamine] (mM)
R² = 0.54
log 10 [putrescine]
R² = 0.66
transpiration (mL/day)
R² = 0.64
log10 CFU per g of fresh weight
[glutamine] (mM)
R² = 0.55
log 10 [putrescine]
R² = 0.51
log10 CFU per g of fresh weight
R² = 0.81
disease index

Figure 6

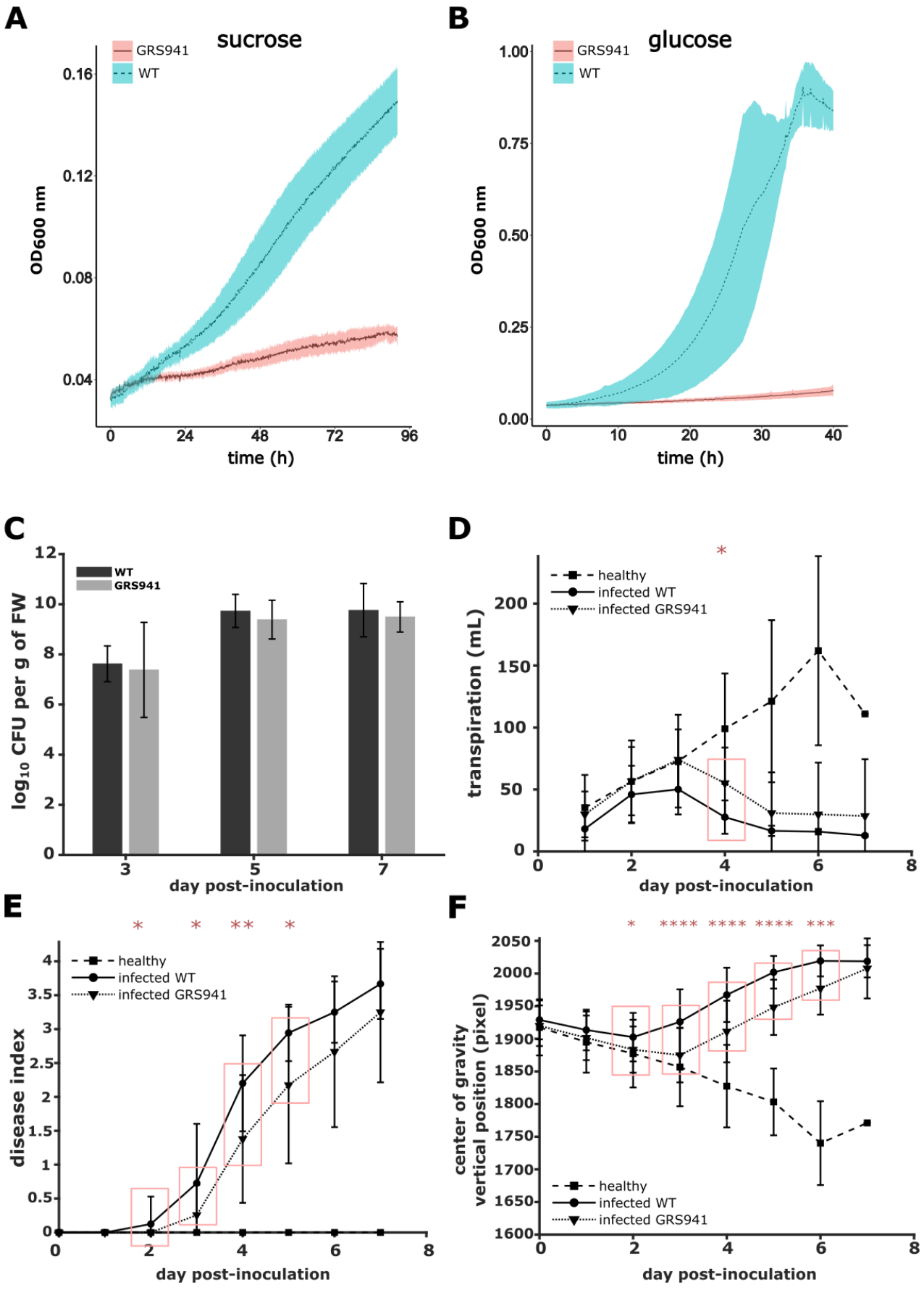
A
sucrose
GRS941
WT
OD600 nm
time (h)
B
glucose
GRS941
WT
OD600 nm
time (h)
C
WT
GRS941
log10 CFU per g of FW
day post-inoculation
D
healthy
infected WT
infected GRS941
transpiration (mL)
day post-inoculation
E
healthy
infected WT
infected GRS941
disease index
day post-inoculation
F
healthy
infected WT
infected GRS941
center of gravity
vertical position (pixel)
day post-inoculation

Figure 7

Table 1. Xylem metabolite content and the impact of *R. solanacearum* infection

Metabolite	**Concentration in healthy plant (mM)**	**Effect of the infection[1]**	**Growth of *R. solanacearum* as sole carbon source[2]**
glutamine	3.29 ± 1.25	decrease	+
asparagine	0.178 ± 0.074	decrease	+
tyrosine	0.022 ± 0.010	putative decrease	NA
glucose	0.010 ± 0.026	putative decrease	+
sucrose	0.028 ± 0.018	putative decrease	+
fumarate	0.004 ± 0.006	putative decrease	+
aspartate	0.015 ± 0.014	no effect	+
phenylalanine	0.035 ± 0.022	no effect	-
leucine	0.088 ± 0.029	no effect	-
lysine	0.123 ± 0.062	no effect	-
glutamic acid	0.020 ± 0.041	no effect	+
threonine	0.062 ± 0.019	putative increase	+
valine	0.083 ± 0.025	putative increase	+
proline	0.066 ± 0.033	putative increase	-
alanine	0.012 ± 0.007	putative increase	+
isoleucine	0.048 ± 0.015	putative increase	-
ethanol	0.203 ± 0.314	putative increase	NA
arginine	0.094 ± 0.051	putative increase	-
3-hydroxybutyric acid	0.005 ± 0.040	putative increase	+
acetate	0.008 ± 0.033	increase	+
putrescine	not detected	appearance	-

Supplementary Figures and Tables

Figure S1. Step-by-step segmentation pipeline.

Are represented the major steps of the segmentation process. The JSON script of this specific pipeline is available as supplementary file 1 and can be uploaded, run and modified using the IPSO-Phen software package available at Github *https://github.com/tpmp-inra/ipso_phen*.

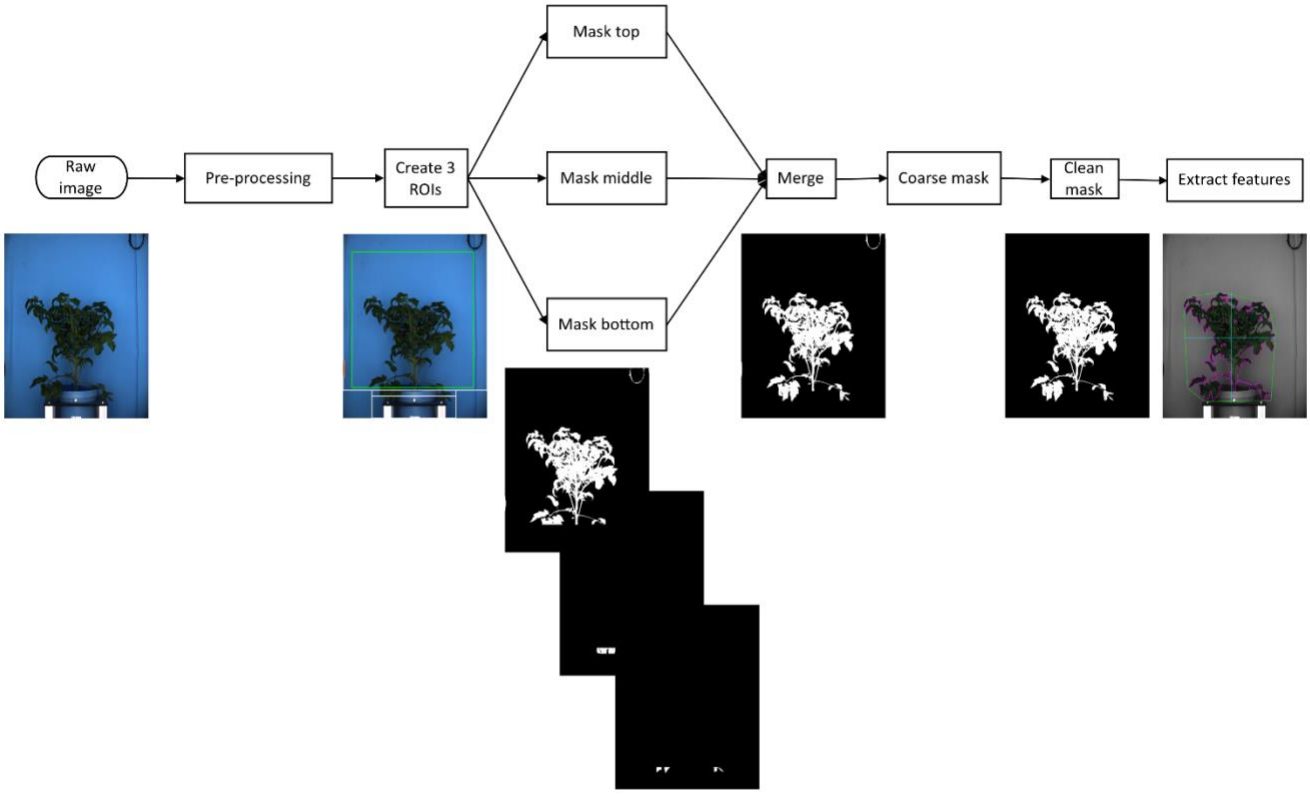

Figure S2. The centroid-y trait (Cy).

The Centroïd-y traitor "Cy" is the y coordinate of the center of gravity of the plant area (Cy is one os the trait extracted as a final step of the image analysis process (see Supplementary figure X0). The origin of the Y axis is set at the top of the image. Plant growth, as an upwards expansion, lowers the Cy value. Bacterial wilt, with leaves dropping and later decaying, increases the Cy value.

Figure S3. Examples of Cy values on healthy and diseased plants.

Two distinctive plant images corresponding to disease index O, or healthy, and diseased (DI=2, 3 or 4) are showed with their respective Cy values (in pixel).

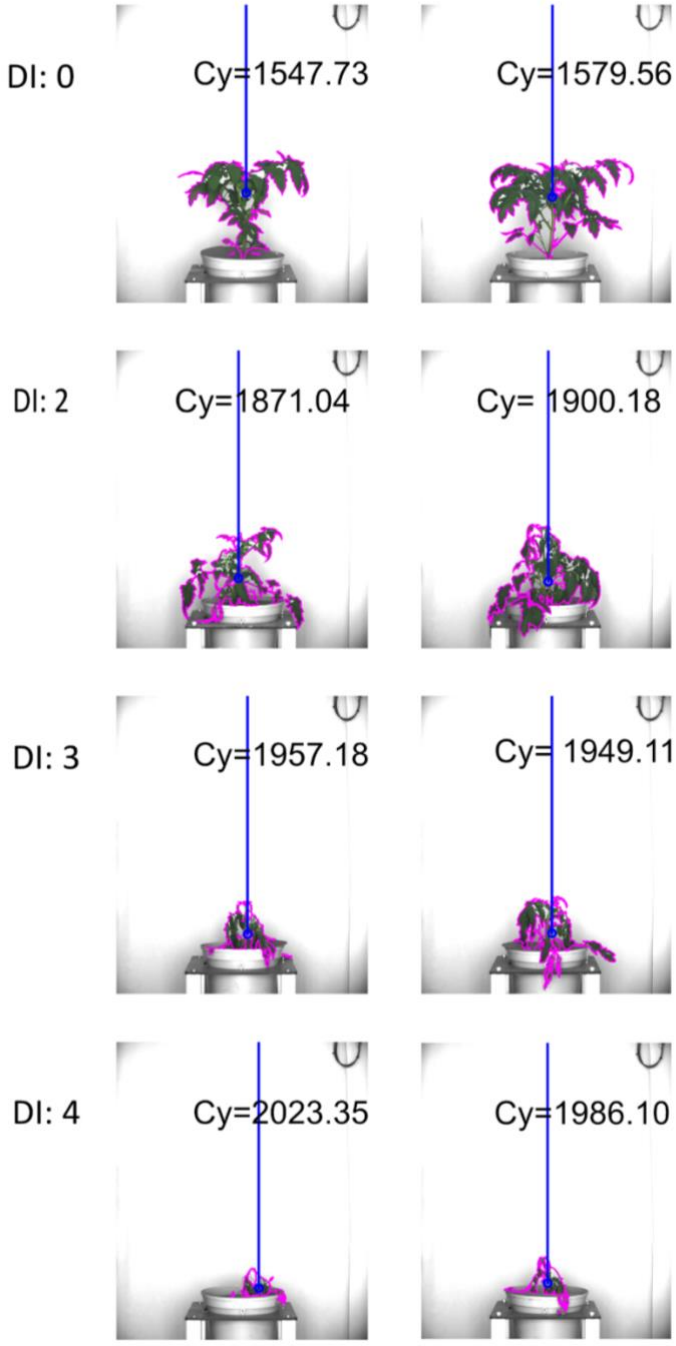

Figure S4. Biological replicate of the physiological measurements.

Impact of *R. solanacearum* colonization on plant physiology (dry weight/transpiration) and monitoring of disease kinetics (disease index), imaging parameters (chlorophyll/center of gravity position) and water content. Chlorophyll content was estimated through RGB values (automatic phenotyping) of plant images as described by Liang et al (Liang et al., 2017). Center of gravity position (vertical) was estimated through plant imaging (automatic phenotyping) with 0 pixel representing the top of the plant. The data presented are from an experiment on 90 plants with at least 3 plants per conditions at each sampling point. Fresh weight and dry weight were used to determine the proportion of water in healthy and infected tissues. Bars indicate standard deviation. Healthy and infected plant data were compared by Wilcoxon-Mann-Whitney test (*: p-value<0.05, **: p-value<0.01, ***: p-value<0.001, ****: p-value <0.0001).

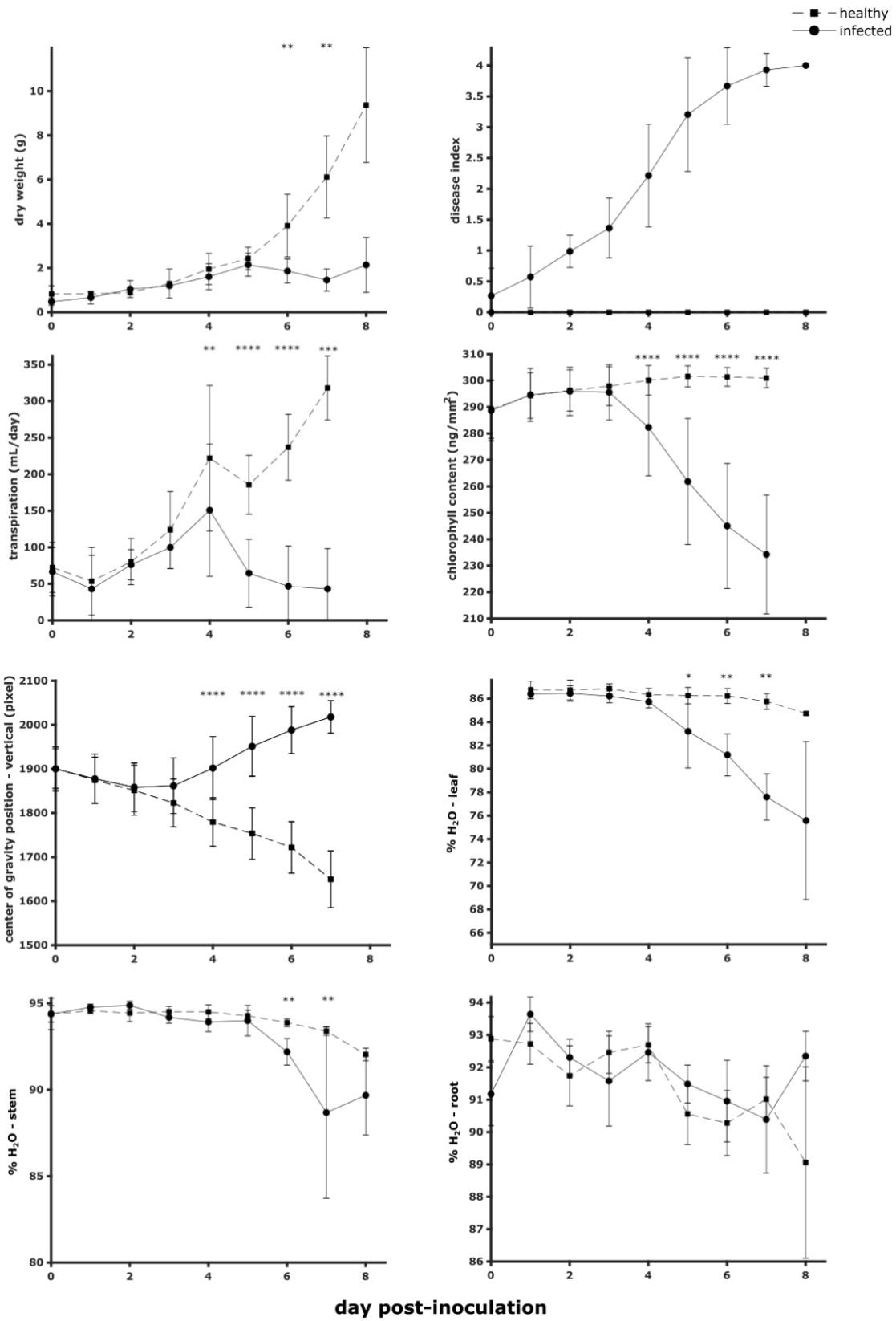

Figure S5. Impact of *R. solanacearum* infection on plant tissues metabolic content.

The mean and standard deviation displayed were obtained after combining the acquired data of the two biological replicates (total of 12 samples for leaf, 10 or 12 for stem, 12 for root at each time point). Healthy and infected plant data were compared by Wilcoxon-Mann-Whitney test (no significant change on the metabolites presented on this figure).

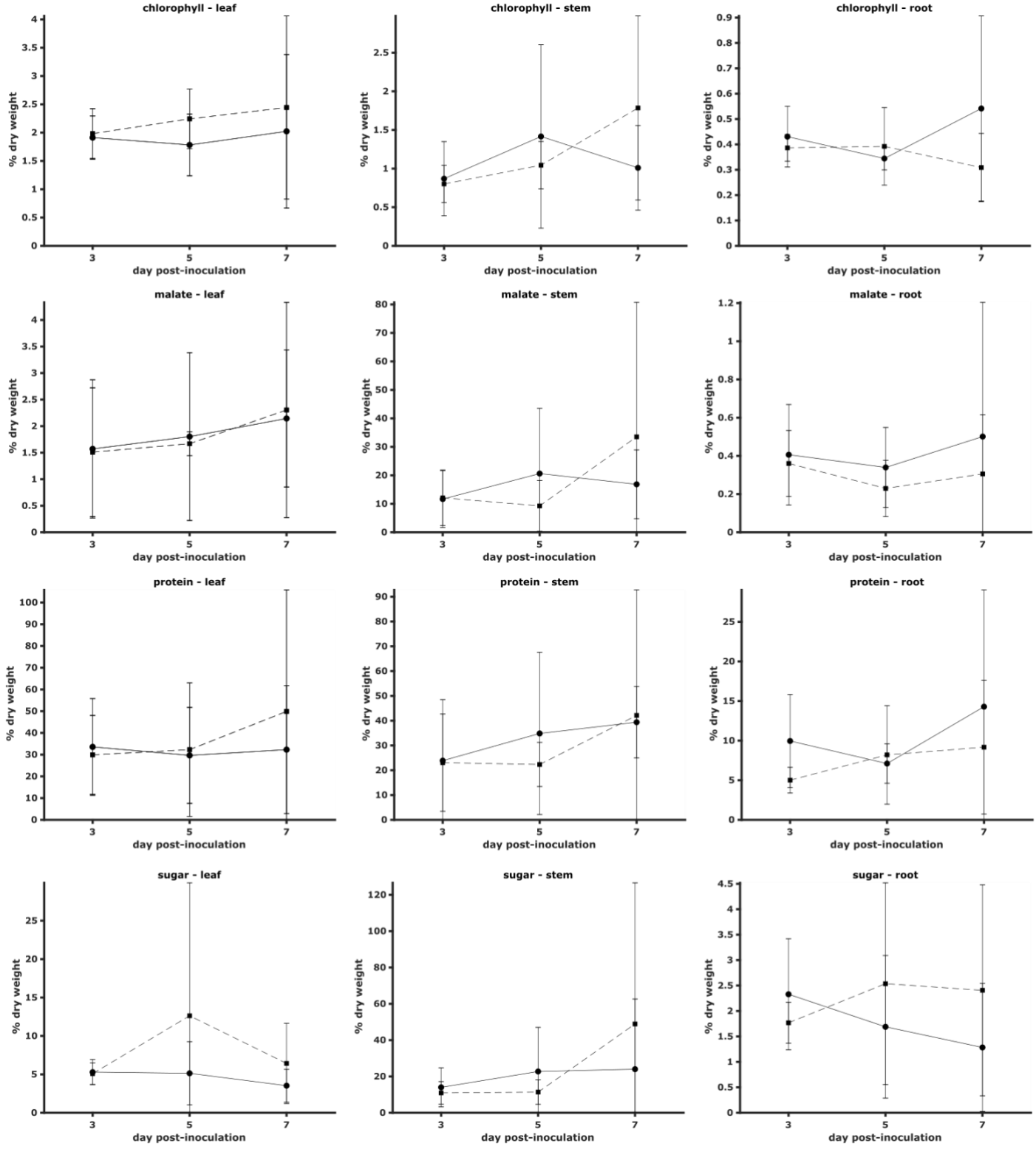

Figure S6. PCA on the biological replicate data: experimental points (A) and variables (B).

As CFU per gram of fresh weight data were not available, infection stage (ni: non-infected, ir_bf_3dpi: infected, sampling before or at 3dpi, ir_af_3dpi: infected, sampling after 3dpi) was mapped on the analyzed data. Similarly to the PCA presented in the Results section, glutamine are the compounds the most correlated with no infection or limited infection stage as it is oriented at the top left (B) which is associated with no or early infection. Oppositely, putrescine and acetate are at bottom right (B) which is associated with late infection. Other compounds associated with late infection include acetate, also noticed in the Results figure as associated with the infection. Other compounds appear to be associated with the infection so as fumarate but this association was not confirmed by the replicate presented in the Results figure.

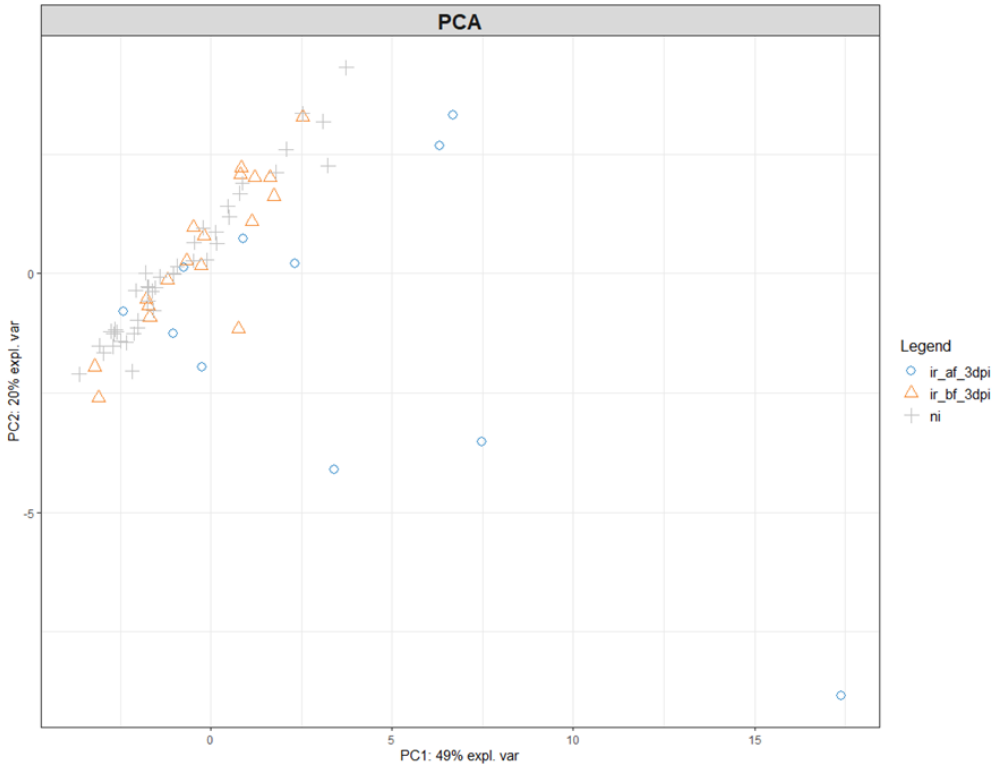

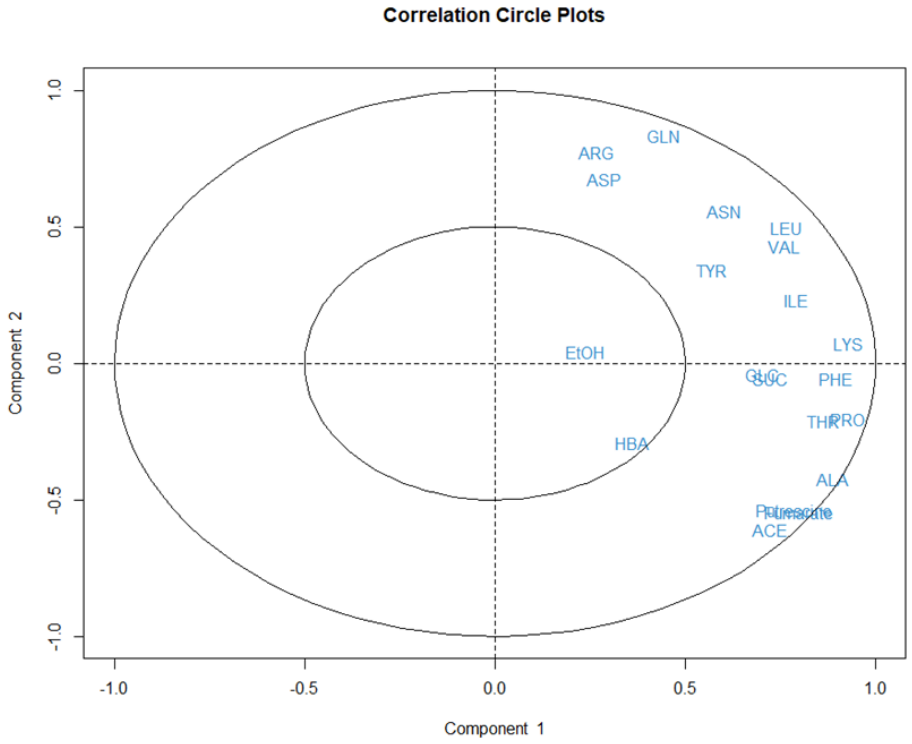

Figure S7. Explained variance of the principal components.

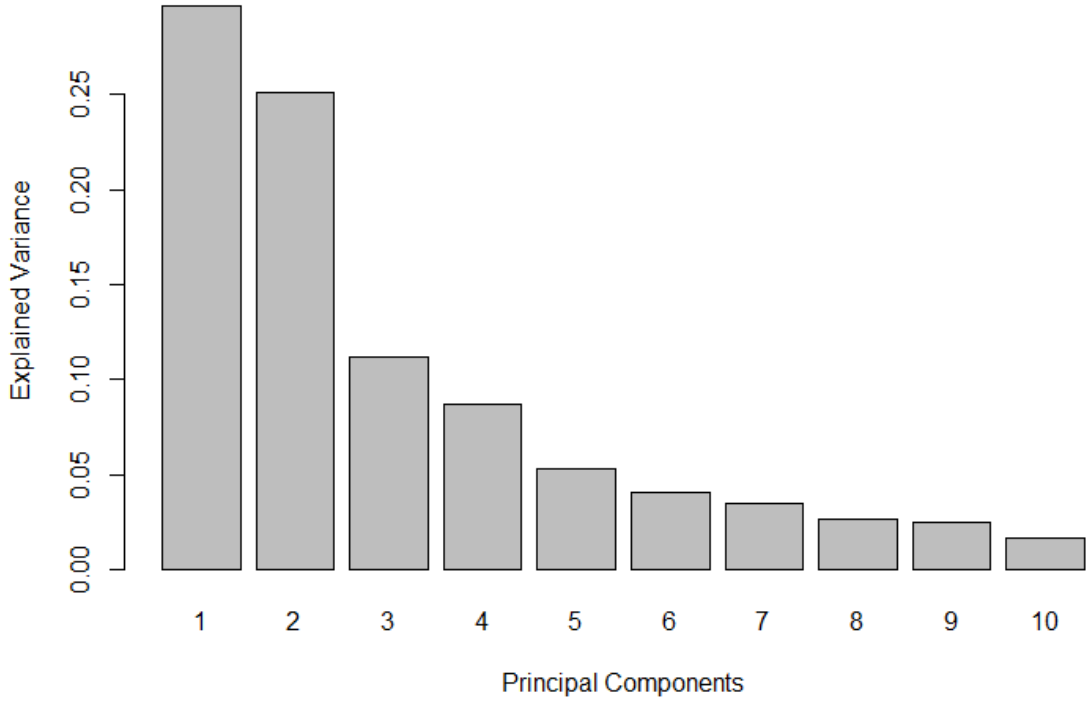

Figure S8. Concentration profiles for alanine and other metabolites with non-statistically significant infection effect.

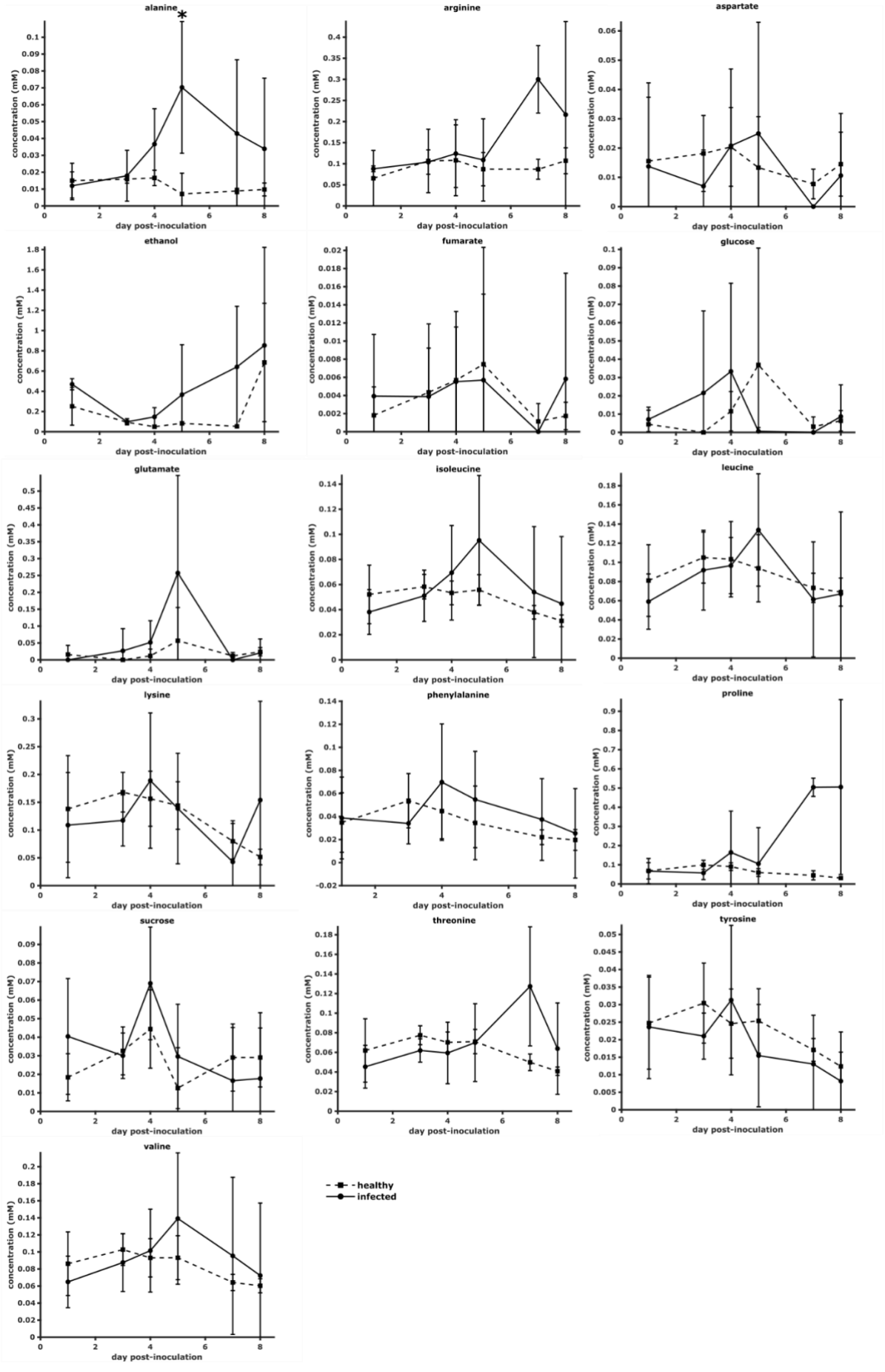
alanine
*
arginine
aspartate
ethanol
fumarate
glucose
glutamate
isoleucine
leucine
lysine
phenylalanine
proline
sucrose
threonine
tyrosine
valine
concentration (mM)
day post-inoculation
healthy
infected

Fig S9. In vitro and in planta phenotyping of R. solanacearum triple mutant strain defective for glucose, sucrose and fructose assimilation.

Growth on minimal medium supplemented with glutamine (A) and sucrose (B) as sole carbon source monitored in microplates with three independent biological replicates. Means and standard deviations are represented by the lines and colored areas, respectively. Plant dry weight (C, F) and bacterial population (H) were determined on at least 9 plants per condition and per day day for infected WT/GRS941 (except 3 at 8 dpi for F) and at least 3 plants per condition and per day for healthy plants. Disease index, transpiration and chlorophyll content (D, E, G) were determined on at least 7 plants per condition and per day for infected WT/GRS941 (except 3 at 8 dpi for E, G) and at least 3 plants per day for healthy plants. E, F, G, H represent an independent experimental repeat, and C, D are complementary figures of the experiment presented in the results section of the article. Means are presented and bars indicate standard-deviation. Infection by wild-type (WT) and GRS941 strains data were compared by Wilcoxon-Mann-Whitney test (*: p-value<0.05, **: p-value<0.01).

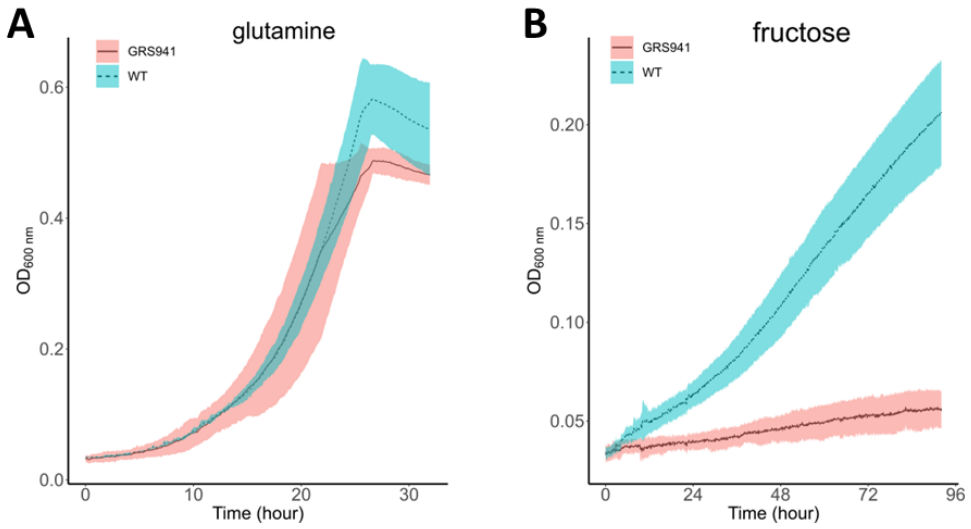
A
glutamine
GRS941
WT
OD600 nm
Time (hour)
B
fructose
GRS941
WT
OD600 nm
Time (hour)

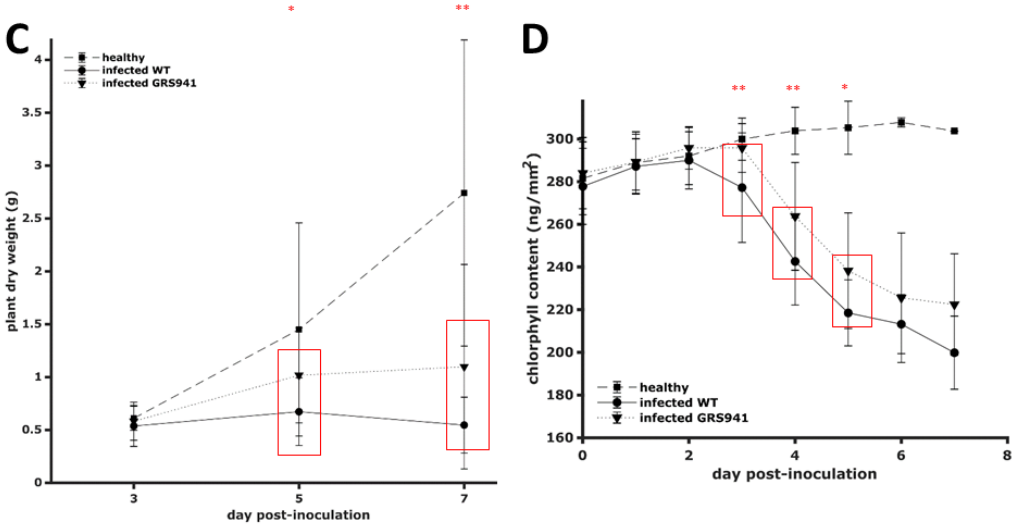
C
healthy
infected WT
infected GRS941
plant dry weight (g)
day post-inoculation
D
chlorphyll content (ng/mm2)
day post-inoculation

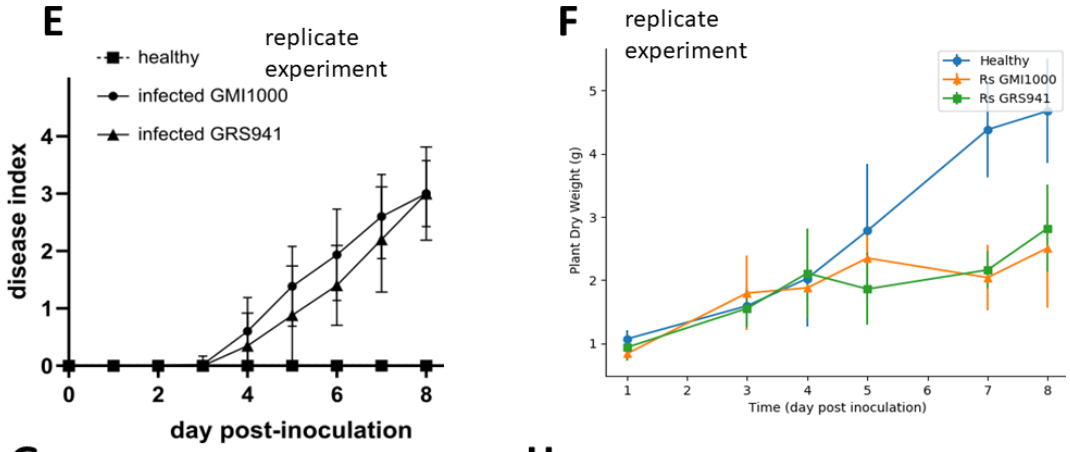
E
replicate
experiment
healthy
infected GMI1000
infected GRS941
disease index
day post-inoculation
F
replicate
experiment
Healthy
Rs GMI1000
Rs GRS941
Plant Dry Weight (g)
Time (day post inoculation)

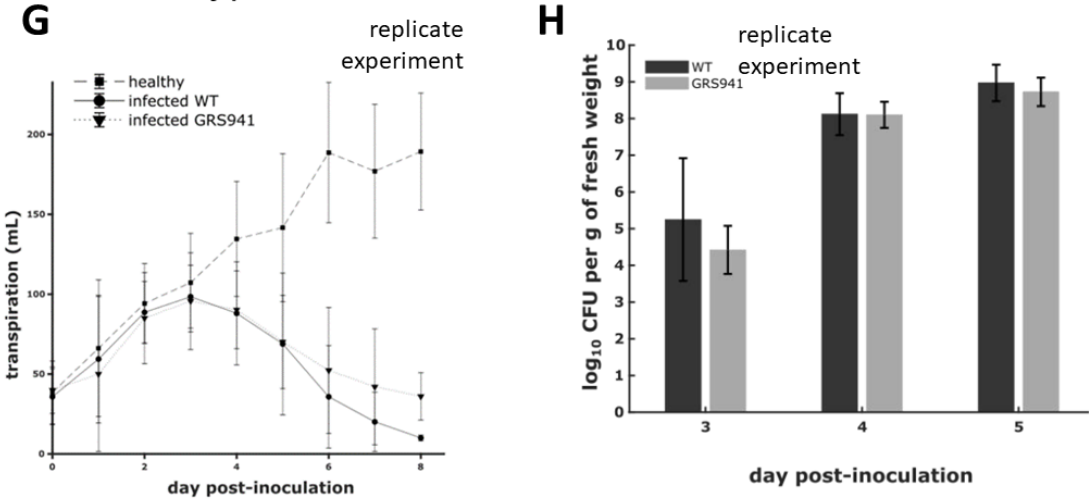
G
replicate
experiment
healthy
infected WT
infected GRS941
transpiration (mL)
day post-inoculation
H
replicate
experiment
WT
GRS941
log10 CFU per g of fresh weight
day post-inoculation

Fig S10. NMR spectrum example.

A. PHE: phenylalanine, TYR: tyrosine, SUC: sucrose, GLC: glucose, ASP: aspartate, ASN: asparagine, GLN: glutamine, GLU: Glutamate, PRO: proline, ARG: arginine, ACE: Acetate, Putr: Putrescine, LYS: lysine, ALA: Alanine, THR: threonine, EtOH: ethanol, 3HB: 3-hydroxybutyric acid, ILE: isoleucine, LEU: leucine, VAL: valine. B and C highlight the difference of spectrum aspects between glutamine and glutamate (or its conjugated acid glutamic acid), and a xylem sample with very few glutamate but high glutamine content: on B, the spectrum profile between 3.7 and 3.8 ppm is different (aspect and number of peaks) and on C, glutamine and glutamate profiles are very different: location and number of group of peaks.

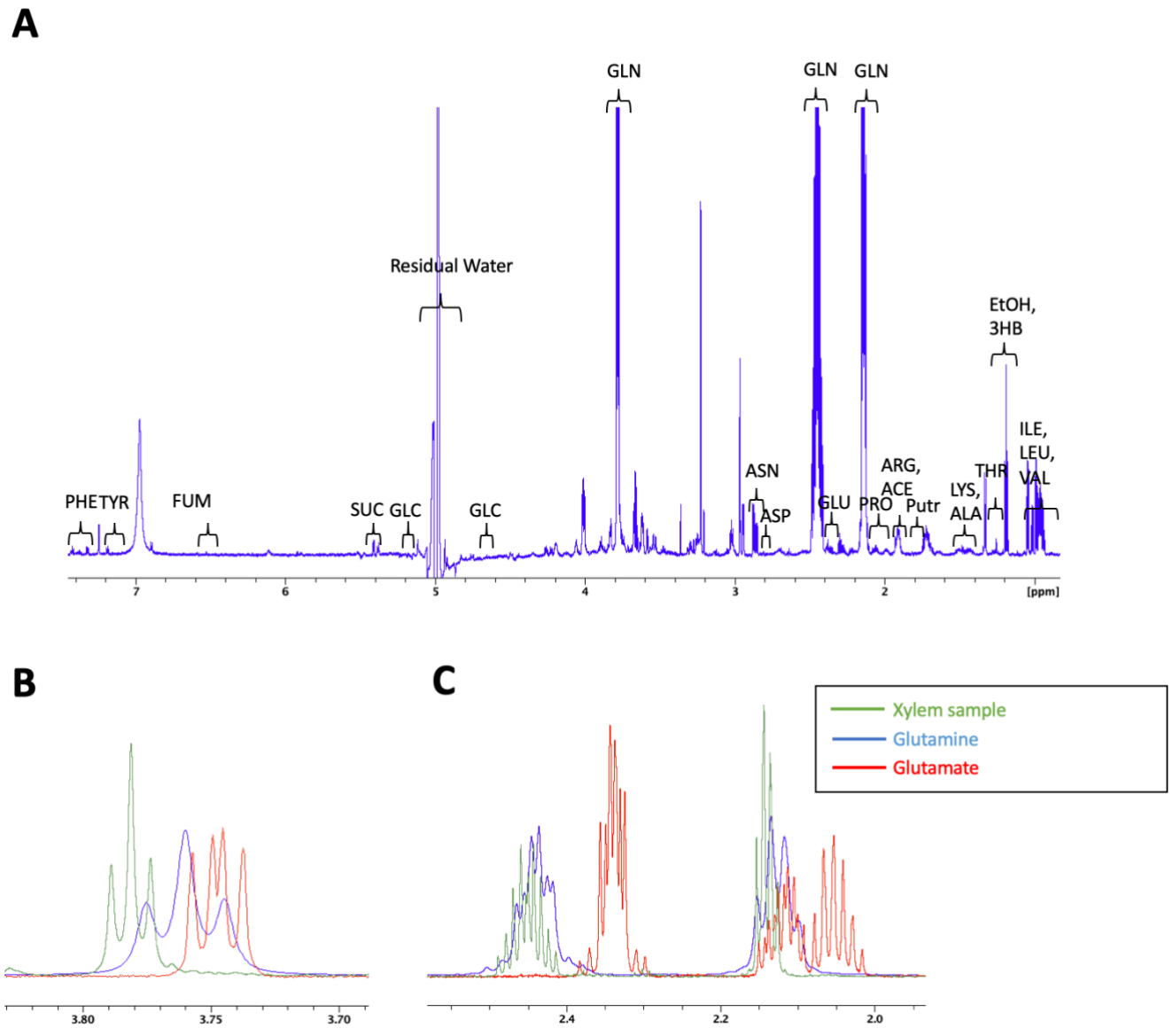

Table S1. Biological replicate of the composition of non-infected xylem.

Metabolite	Concentration in healthy plant (mM)
glutamine	3.259 ± 1.633
asparagine	0.143 ± 0.078
tyrosine	0.025 ± 0.007
glucose	0.031 ± 0.058
sucrose	0.070 ± 0.052
fumarate	0.002 ± 0.003
aspartate	0.017 ± 0.014
phenylalanine	0.029 ± 0.011
leucine	0.081 ± 0.029
valine	0.076 ± 0.026
proline	0.118 ± 0.058
lysine	0.163 ± 0.052
isoleucine	0.052 ± 0.017
arginine	0.132 ± 0.051
ethanol	0.771 ± 0.910
putrescine	not detected
threonine	0.058 ± 0.019
glutamate	not detected
acetate	not detected
3-hydroxybutyric acid	not detected
alanine	0.021 ± 0.007

Table S2. Loading weights on the second component of the PCA. (update)

Metabolite	Loading weight
PUTR	0.401
GLN	-0.350
ACE	0.339
ASN	-0.325
PRO	0.300
ARG	0.242
ALA	0.242
HBA	0.2309
TYR	-0.217
THR	0.212
SUC	-0.177
GLC	-0.169
ILE	0.146
ETOH	0.116
VAL	0.116
FUM	-0.113
ASP	-0.091

GLU	0.086
PHE	-0.075
LEU	0.020

Generation of *R. solanacearum* triple mutant strain defective for glucose, sucrose and fructose assimilation

Strain GRS941 was engineered by cumulating deletions in the glucose transport operon (RSp1632-RSp1635), the sucrose assimilation operon (RSp1280-RSp1286) and the fructose transport operon (RSc2861-RSc2863).

An unmarked internal deletion in of the glucose transport operon (ΔRSp1632-RSp1635) gene was created using the *sacB*-mediated counter selection system (Schäfer et al., 1994). Briefly, upstream (RSp1632) and downstream (RSp1635) regions were PCR amplified using the primer pairs 1632A/1632B and 1635C/1635D, respectively, and cloned into the *Eco*RI-*Hin*dIII-digested pk18mobsacb to generate pK18-ΔRSp1632/1635 (listed below). The circularized plasmid was recombined in strain GMI1000 through natural transformation (Perrier et al., 2018).

Kanamycin-resistant and sucrose-sensitive recombinant clones were first selected and in a second step, after overnight culture in BG medium (Plener et al., 2010), kanamycin-sensitive and sucrose-resistant clones were screened by PCR using the primer pair 1632A/1635D to identify a ΔRSp1632-RSp1635 recombinant. The resulting mutant was named GRS903.

A deletion of the RSp1280-RSp1286 region was created by double recombination using a selectable antibiotic interposon cassette from pHP45 (Prentki & Krisch, 1984): upstream (RSp1286) and downstream (RSp1280) regions were PCR amplified using the primer pairs 1280R1 /1280Sc and ScrR-Xba/ScrR-R1, respectively, cloned in the pGEMT vector (Promega), and then the Ω interposon was inserted in the unique *Eco*RI site. The resulting plasmid pSG804 was recombined in strain GRS903 through natural transformation as described above, and spectinomycin-resistant clones were selected and PCR-validated, yielding strain GRS936.

A deletion of the *fruBKA* operon (RSc2861-RSc2863) was created by double recombination using the selectable integrative plasmid pCM184 (Marx & Lindstrom, 2002): upstream (RSc2861) and downstream (RSc2863) regions were PCR amplified using the primer pairs fru-bgl-2/fru-nde-2 and fru-Sac2/fru-Sc1, respectively, and cloned in pCM184 as *Bgl*II-*Nde*I and *Sac*II-*Sac*I inserts, respectively. This recombinant plasmid, pSG753, was recombined in strain GRS936 through natural transformation as described above, then gentamycin-resistant clones were selected and PCR-validated, yielding strain GRS941.

List of oligonucleotides used in this study

1632A	GAATTCAGGAGACAGTCCATGGAGCTC
1632B	TCTAGATCAGCGCGCCGGTGGTG
1635C	TCTAGATCTCCGTCACGGGCATG
1635D	AAGCTTGACGATCATCTGCCACG
1280R1	GCCTGCTCACGCGCCCGGAGG
1280Sc	GAGCTCGCCCAACAAGTTCGAG
ScrR-Xba	TCTAGATCAATTCGTACACCAC
ScrR-R1	GAATTCAACCTCGGCGCTATTGC
fru-bgl-2	AGATCTGCTGGTGCGGCCGAACAGC
fru-nde-2	CATATGTGCTCGTCCGACTGCG
fru-Sac2	CTGGCGCGCATGCTGGACAG
fru-Sc1	GAGCTCGGCGTGTAGACCTGGC

References

Marx CJ, Lidstrom ME (2002) Broad-host-range cre-lox system for antibiotic marker recycling in gram-negative bacteria. Biotechniques 33:1062-1067. doi: 10.2144/02335rr01.

Perrier A, Barberis P, Genin S (2018) Introduction of genetic material in *Ralstonia solanacearum* through natural transformation and conjugation. Methods Mol Biol. 1734:201-207. doi: 10.1007/978-1-4939-7604-1_16.

Plener L, Manfredi P, Valls M, Genin S (2010) PrhG, a transcriptional regulator responding to growth conditions, is involved in the control of the type III secretion system regulon in *Ralstonia solanacearum*. J Bacteriol. 192:1011-1019. doi: 10.1128/JB.01189-09.

Prentki P, Krisch HM (1984) *In vitro* insertional mutagenesis with a selectable DNA fragment. Gene 29:303-313. doi: 10.1016/0378-1119(84)90059-3.

Schäfer A, Tauch A, Jäger W, Kalinowski J, Thierbach G, Pühler A (1994) Small mobilizable multi-purpose cloning vectors derived from the *Escherichia coli* plasmids pK18 and pK19: selection of defined deletions in the chromosome of *Corynebacterium glutamicum*. Gene 145: 69–73.